Technical report on

TSUNAMI INUNDATION MODELLING FOR THE EAST COAST OF TASMANIA

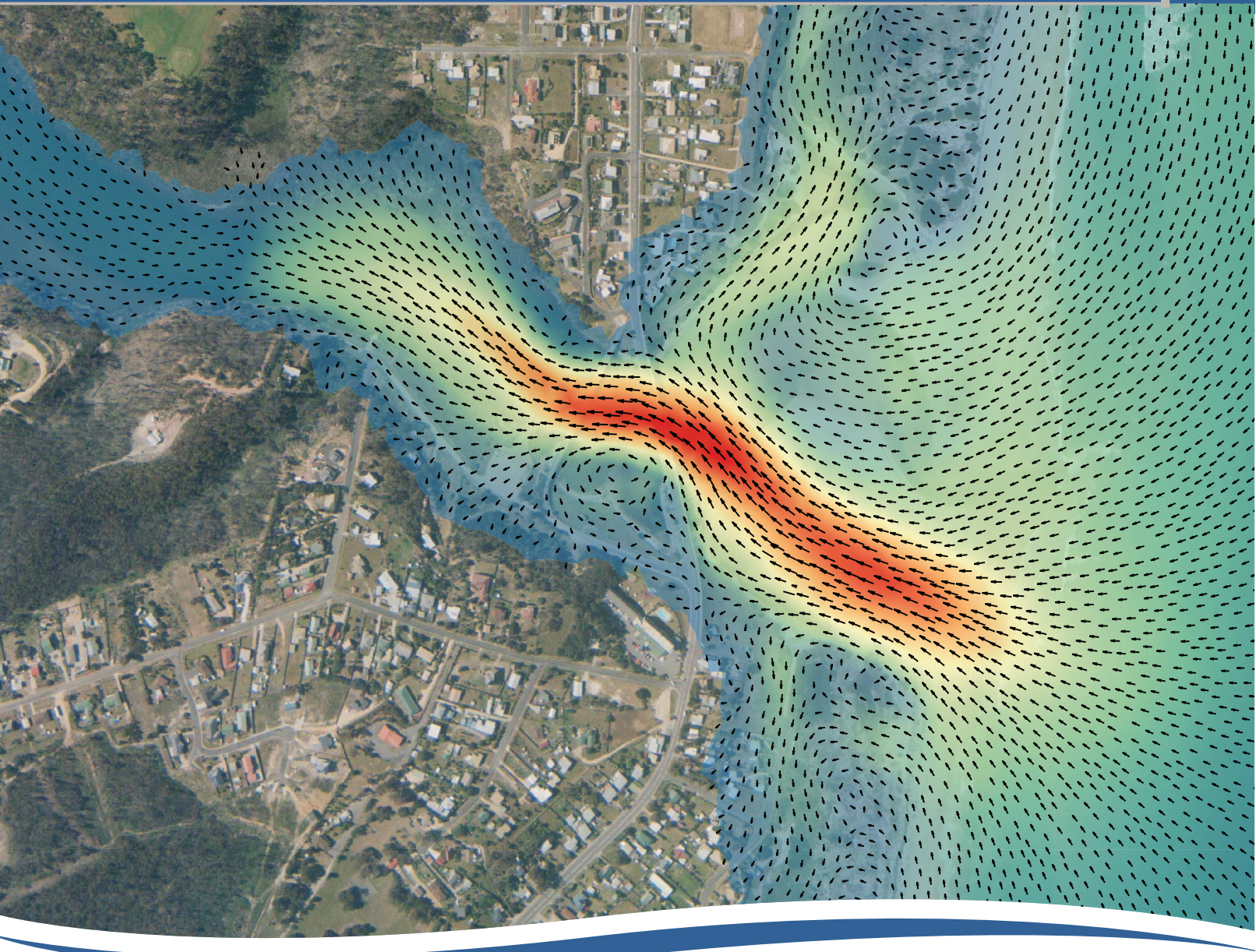

Geological Survey Branch
Mineral Resources Tasmania
Department of State Growth

Tasmanian Government

Technical report on

TSUNAMI INUNDATION MODELLING FOR THE EAST COAST OF TASMANIA

FEBRUARY 2022

Claire L. Kain

Geological Survey Branch
Mineral Resources Tasmania

Cover image: *Snapshot of the simulated tsunami momentum as the tsunami travels into the Scamander River mouth*

Tasmanian Geological Survey Report
TR25

CONTENTS

EXECUTIVE SUMMARY	3
INTRODUCTION	4
Overview of tsunami dynamics and hazard	5
Scope and report structure	6
METHODS	7
Tsunami scenario selection from the 2018 PTHA database	7
Input data and model implementation	10
Boundary conditions	10
Model resolution and mesh structure	10
Elevation model	11
Manning's *n* surface roughness model	12
Dune erosion zones	13
Simulation using ANUGA	14
Data processing	14
Model validation and sensitivity testing	14
RESULTS	16
General overview	16
Location-specific results	20
Swansea - Freycinet Peninsula - Bicheno (Maps 1-18)	20
Douglas River - Seymour - Lagoons Beach (Maps 19 - 23)	24
Four Mile Creek - Falmouth - Scamander - Beaumaris (Maps 24 - 29	26
St Helens - Binalong Bay - Larapuna - Bay of Fires (Maps 30 - 38)	30
Ansons Bay - Stumpys Bay (Maps 39 - 43)	33
DISCUSSION	35
Comparison between scenarios and source zones	35
Limitations and recommendations	36
SUMMARY AND CONCLUSIONS	37
ACKNOWLEDGEMENTS	38
REFERENCES	38
GLOSSARY	41
LIST OF APPENDICES	42
APPENDIX 1. POTENTIAL TSUNAMI IMPACTS ON INFRASTRUCTURE	43

EXECUTIVE SUMMARY

Tasmania's east coast is exposed to tsunamis originating from a range of sources around the Pacific Ocean, with a minimum travel time of approximately 2 hours. The 2016 Tasmanian State Natural Disaster Risk Assessment (TSNDRA) recognised tsunami as a hazard with a low probability, but potentially catastrophic consequences, and previous tsunami modelling studies suggest that south east Tasmania could be significantly impacted by a large tsunami (Average Recurrence Interval [ARI]: 13 000 years).

This project extends the tsunami inundation modelling to the east coast of Tasmania, with funding provided by the Natural Disaster Risk Reduction Grants Program (NDRRGP). This report, and accompanying data, have been prepared for the Tasmania State Emergency Service by Mineral Resources Tasmania. The objective is to perform tsunami inundation modelling of a critical-but-credible earthquake/tsunami/high-tide scenario for three source zones (Puysegur Trench, Tonga-Kermadec Trench, and New Hebrides Trench) and perform deterministic exposure mapping for vulnerable locations. The model domain extends from Swansea to Ansons Bay, covering a total of 13 000 km^2 and 300 linear kilometres of coastline.

Modelling was undertaken using the two-dimensional ANUGA hydrodynamic modelling library (Nielsen et al., 2005; Roberts et al., 2019), applying a variable resolution model on an unstructured triangular mesh. Structures and land cover were accounted for using a variable surface roughness model. Boundary condition data were obtained from the 2018 Probabilistic Tsunami Hazard Assessment database (Davies and Griffin, 2018), and water level was set at highest astronomical tide. A total of 20 scenarios were modelled, with ARI for all but two scenarios ranging from 8 000 to 16 000 years. The results of four designated scenarios (all approximate ARI 11 000 years) were analysed in detail.

Simulated tsunami inundation was greatest in east-facing open coast areas, with maximum tsunami wave amplitude reaching > 7 m above mean sea level (AMSL) in the south and 5 m AMSL in the north of the model domain. Onshore run-up height consistently reached 7 m AMSL in exposed locations. In many areas, modelled run-up was tightly controlled by the topography so that inundation footprints were similar for all scenarios. However, simulated flow depths were generally greater for larger tsunamis. Post-earthquake tsunami arrival times for Puysegur scenarios were approximately 2 hours 10 minutes, whereas arrival times for Tonga-Kermadec and New Hebrides tsunamis were 5 hours 25 minutes and 5 hours 10 minutes, respectively.

The most affected human settlement areas include Scamander and Douglas River, with St Helens, Beaumaris and Bicheno also experiencing some impact to low-lying properties and infrastructure. Many settlements are situated > 8 m AMSL and were unaffected in the simulations, beyond some inundation of beaches and coastal reserves. Results indicate that the A3 Tasman Highway would be flooded or washed out at several locations, particularly in the south of the study area. In comparison with the south east Tasmania modelling results, modelled maximum run-ups and flow depths for similarly exposed locations on the east coast were generally less severe.

Puysegur Trench tsunamis tend to result in slightly greater wave amplitudes, run-up heights and flow depths than other source zones in the south of the model domain, with impacts decreasing northwards along the east coast. However, New Hebrides tsunamis tend to have greater impacts than Puysegur tsunamis in the north of the study area, with maximum wave amplitudes and run-up heights decreasing slightly southwards. Tsunamis generated along the Tonga-Kermadec Trench show no spatial trends across the model domain.

This project is intended to explore the impacts of a critical-but-credible tsunami scenario, and the modelling was performed using the best available data. A full tsunami risk assessment is outside the scope of this project and would require many more scenarios to provide a more complete view of tsunami hazard, alongside a full analysis of vulnerability and exposure. Changes in elevation and land cover may also affect the applicability of the results to future events. It is important to note that the interaction of tsunami waves with tides and currents was not captured as the model was not run with a dynamic tide. The impacts of climate change and sea level rise were not modelled; however, sea level rise could increase tsunami flow depths in low-lying areas and result in a greater susceptibility to inundation in the future.

Alongside this report, the project outputs include a tsunami inundation map series for each of the four designated tsunami scenarios, covering 43 coastal communities and important reserve areas. These outputs are intended to assist emergency managers in understanding potential tsunami hazard along Tasmania's east coast.

INTRODUCTION

Following the Tasmanian State Natural Disaster Risk Assessment (TSNDRA) in 2016, tsunami was recognised as a hazard with a low probability, but potentially catastrophic consequence for Tasmania (Department of Police, Fire and Emergency Management, 2017). The east coast of the island is exposed to tsunamis originating from several regions around the Pacific Ocean, with travel times ranging from 2 hours post-earthquake, to upwards of 12 hours.

Tsunami hazard has been poorly understood in Tasmania until recently, due to the infrequent nature of destructive tsunami events and the comparatively short timeframe of written historical records. No large tsunamis have occurred in European-era recorded history, but several smaller tsunamis have been documented, and a global tsunami in 1868 caused notable damage at several locations in south east Tasmania (Keith, 1868; Morris and Mazengarb, 2009). On a longer timescale, geological evidence has been found in south east Tasmania for three significant tsunami events within the last 4000 years (Clark et al., 2011).

Numerical modelling of tsunamis can provide a means of understanding the magnitude, variability and relative timing of their impacts and subsequently assessing the vulnerability of coastal communities and infrastructure. However, it is important to remember that modelling is a best approximation of reality, and results may change with improvements in scientific understanding, technology and input data. It is particularly difficult to calculate the return intervals of large tsunamis, and considerable uncertainties exist in these magnitude-frequency estimates (AIDR 2018; Davies and Griffin, 2018).

Two previous tsunami modelling studies have been undertaken for south east Tasmania. In 2009, Geoscience Australia (GA) produced the first model, which suggested that parts of the coastline could be significantly impacted by a large tsunami generated off New Zealand's south west coast (Van Putten et al., 2009). Emergency managers sought a better understanding of the modelled hazard, and in 2014 Mineral Resources Tasmania (MRT) was awarded funding from the Natural Disaster Resilience Grant Programme to re-model GA's critical-but-credible tsunami scenario using new high-resolution input data (Kain et al., 2018; Kain et al., 2019). The MRT study mapped potential coastal inundation for 71 coastal areas and provided a maritime hazard assessment for Hobart Port infrastructure and operations. The results of this study were well received by the Emergency Management community, who requested that the modelling be extended to other vulnerable coastal areas.

The east coast of Tasmania was selected for the current study (Figure 1) because it is exposed to tsunamis from several key source zones, including Puysegur Trench, Tonga-Kermadec Trench and New Hebrides Trench (Figure 2). The study domain extends from Swansea to Ansons Bay, covering an area of 13 000 km^2 (Figure 1) with a population of approximately 7500 (Australian Bureau of Statistics, 2016).

The purpose of this study is to understand the potential impacts of a critical-but-credible earthquake/tsunami/high-tide scenario from each of the aforementioned source zones, in terms of flooding extents, flow (inundation) depths and offshore velocities. Alongside this technical report, the project outputs include two map series sets that document the flooding footprints for 43 key coastal locations and will be used by stakeholders to inform emergency management policies and plans.

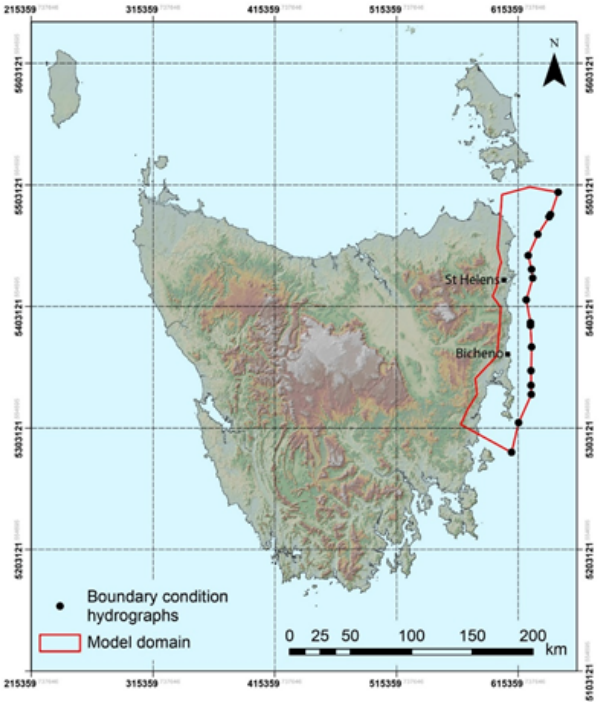

FIGURE 1: Location of the study area and boundary condition hydrographs.

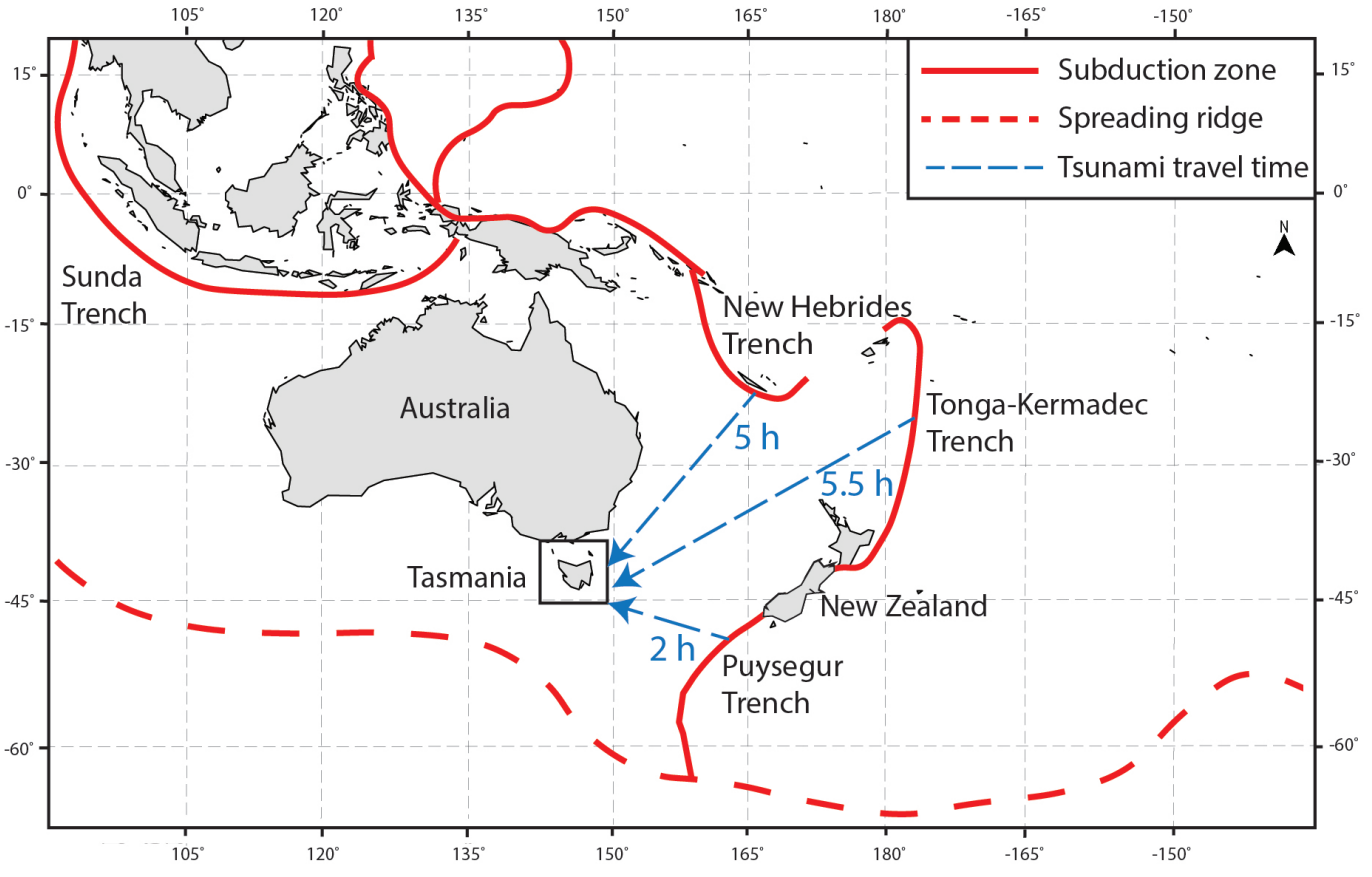

FIGURE 2: Location map of tsunami subduction source zones around Australia. Approximate tsunami travel times to Tasmania from the modelled source zones are shown in blue.

Overview of tsunami dynamics and hazard

Tsunamis are transient wave motions that result from ocean water displacement, most commonly caused by events such as earthquakes, submarine volcanic eruptions, or landslides that occur either underwater or enter into water. They are characterised by a series of waves with periods ranging from minutes to hours. Tsunamis inundate the shore as a steady or rapid increase in water level, a fast-moving bore, or sometimes large breaking waves. The first wave may not be the largest, and recurring inundation and strong or unusual currents may persist for several days.

Earthquake-generated tsunamis are most commonly caused by subduction zone earthquakes and may lead to inundation and damage in locations far from their source (e.g. those listed in Satake et al., 2020). For example, a tsunami generated off South America in 1868 resulted in fatalities and damage as far away as New Zealand and Tasmania. In deep ocean areas, tsunami waves travel at speeds of around 800 km hr^{-1} and have wave amplitudes of only a few centimetres. As the waves encounter shallower water they slow down, become closer together and increase in amplitude. The tsunami may arrive as a leading elevation wave (initial rise in water level) or leading depression wave (initial drawback of water), depending on the orientation of the coastline with respect to the geometry of the fault rupture.

Tsunami behaviour in the nearshore is variable, and wave energy may be amplified or attenuated depending on the local bathymetry, coastline geometry, and seafloor or surface cover. Although the offshore wave periods are long, the water level usually fluctuates more frequently and unpredictably at the shoreline, due to wave interference, reflection and interactions with coastal landforms.

Localised tsunami amplification has been commonly observed on complex or non-linear coasts, where waves can be focused by curved embayments or offshore features such as submarine canyons. These localised amplifications may cause wave heights and run-up elevations that are disproportionate to the size of the tsunami at a regional scale.

Tsunamis affect both the natural and anthropogenic environment (Tasmanian context detailed in White et al., 2016). Direct anthropogenic impacts may include damage to buildings and infrastructure, potential for injury and loss of life, or saline incursion and erosion of stormwater, sewerage and water links. Longer term effects may include loss of amenity and environmental value, economic loss, and injury or mental health implications. Erosion of beaches and river/estuary channels can be expected, alongside destruction of vegetation and salinity impacts on arable land and other vegetation in inundated areas.

Scope and report structure

The purpose of this project is to investigate a reasonable critical-but-credible tsunami scenario, which was defined as an event with a 10 000 year average recurrence interval (ARI). Twenty scenarios were modelled around this defining parameter, in order to explore the implications of different source zones and tsunami characteristics on nearshore impacts. Four reference scenarios were then selected for more detailed analysis and presentation. These scenarios were chosen to represent the source zones that contribute most to Tasmania's tsunami risk. It is important to note that, although this study provides information on the impacts from severe tsunamis, the results do not constitute a risk assessment. These outputs are intended to assist emergency managers in understanding potential tsunami hazard along Tasmania's east coast.

This report summarises the methods and results of the tsunami modelling for the east coast of Tasmania and examines the implications of these results. Appendix 1 contains a summary table of potential tsunami impacts and asset damage likelihood based on water depth. This table provides generalised advice and is not specific to Tasmanian data or environments. The primary outputs of this study include two 1:10 000 scale map series. The first shows the maximum flow depths, run-up limits and nearshore velocities for a reasonable maximum credible Puysegur tsunami scenario across 43 coastal communities and reserve areas (Appendix 2). The second shows the inundation footprints for all 20 scenarios across the same locations (Appendix 3). Time series data and geospatial outputs are also provided for all 20 scenarios (Appendix 4), which includes raster and vector outputs of maximum stage (water surface elevation), flow depth, run-up limits and velocities. Selected video animations of the Puysegur scenario are given for key sites in Appendix 5. Appendix 6 contains a vector layer showing locations where one or more of the modelled tsunamis floods the A3 Tasman Highway. An archive of the modelling and post-processing scripts is supplied in Appendix 7, along with a copy of the input data. A glossary of key terms is presented on page 33.

METHODS

The methodological framework for this study was based on the processes developed for the South East Tasmania tsunami modelling project (Kain et al., 2018), with some changes made to the modelling strategy to include a wider range of tsunami source zones. The methods are detailed in the following subsections.

Tsunami scenario selection from the 2018 Australian Probabalistic Tsunami Hazard Assessment database

The 2018 Australian Probabilistic Tsunami Hazard Assessment (PTHA) (Davies and Griffin, 2018) details the offshore tsunami hazard around Australia and provides deep-water data from hundreds of thousands of modelled tsunami scenarios for a network of hazard points. The PTHA 2018 does not assess the nearshore tsunami hazard or the risk for coastal communities, but the data can be used as inputs to develop local or regional-scale inundation models.

For each hazard point, the PTHA provides deep-water tsunami return period curves, which define the maximum tsunami amplitude for a given recurrence interval at the specified point (e.g. Figure 3). This amplitude-exceedance rate relationship is calculated as a sum across all PTHA scenarios and source zones, so the probability of a tsunami of the designated exceedance rate occurring from a particular source zone (e.g. Puysegur or Tonga-Kermadec) will be less. To better understand this relationship, and the importance of each source zone at a given location, the hazard point assessment also includes a spatial hazard deaggregation, which defines the proportion of the hazard associated with each subduction source zone for a given tsunami amplitude (e.g. Figure 4). For example, Figure 4c shows that for an ARI 10 000 year tsunami (based on maximum stage at a hazard point off Eastern Tasmania), there is a greater probability of it originating from the Tonga-Kermadec Trench (exceedance rate of 0.000045 events per year or ARI of 22 000 years), or the Puysegur Trench (exceedance rate of 0.000043 events per year or ARI of 23 000 years), than other possible source zones. When these probabilities are summed across all source zones, the probability of maximum stage exceedance equals 0.00001 or

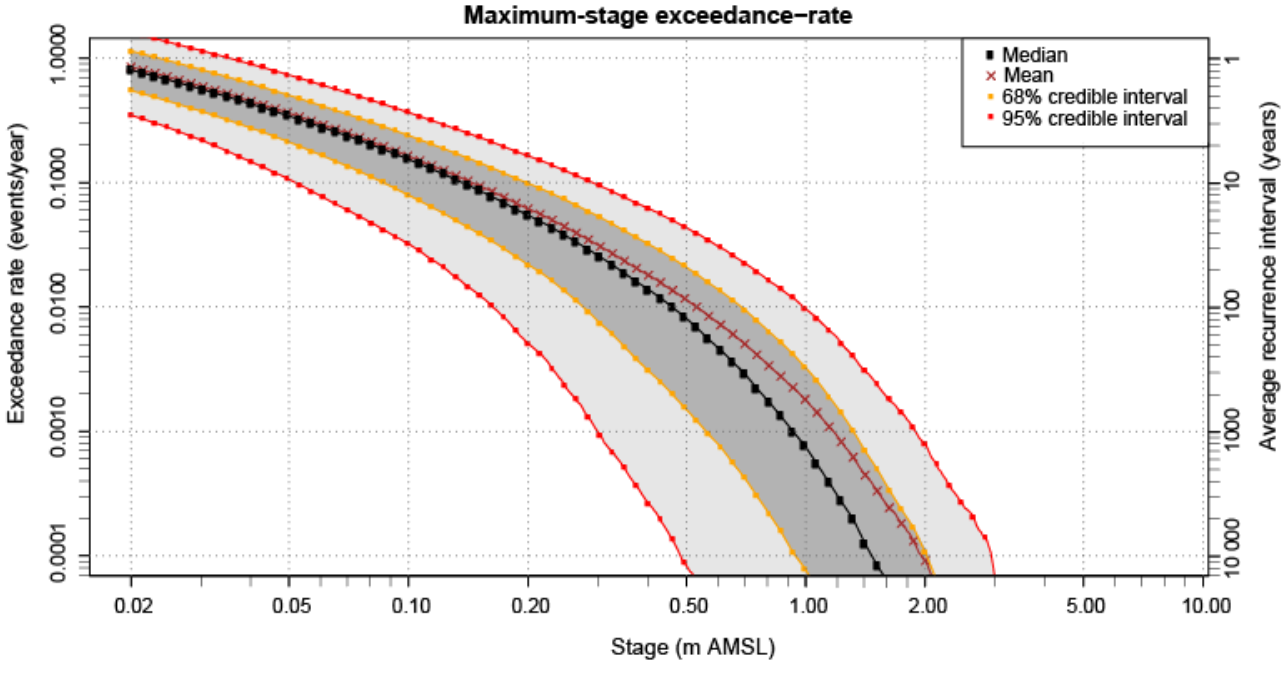

FIGURE 3: Plot of maximum-stage exceedance rates for PTHA Hazard Point 1552.1, which is located off the coast of Scamander where water depth is 103 m (at the model domain boundary in the central part of the study area). This is the same hazard point that is represented in Figure 4b.

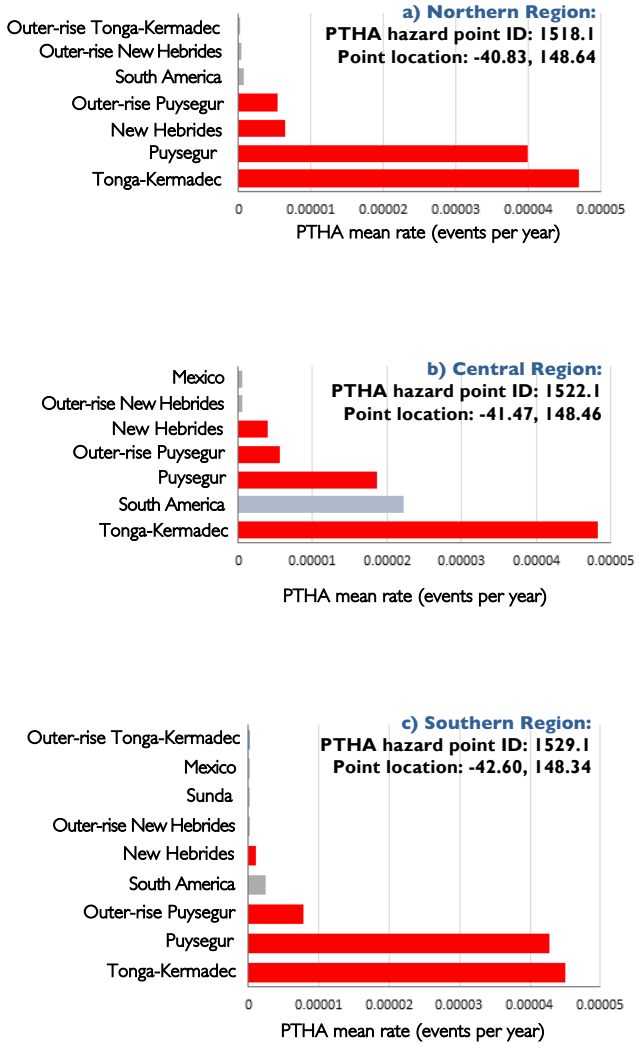

FIGURE 4: Region-specific spatial hazard deaggregation for an ARI 10 000 year tsunami. a) North, b) Central, c) South. These plots describe the proportion of the hazard attributed to different subduction source zones. Source zones modelled in this study are highlighted in red.

Right: Hazard point locations.

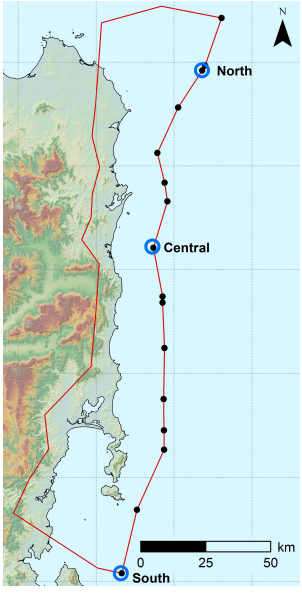

ARI 10 000 years. Users should note that because the recurrence interval is calculated from maximum stage values at the 100 m depth contour (i.e. offshore), this may not correspond exactly to the equivalent ARI tsunami inundation extent on land.

The regional tsunami hazard for the east coast of Tasmania was initially explored for three PTHA hazard points at the 100 m depth contour, located in the southern, central and northern parts of the model domain (Figure 4). The maximum stage for a given ARI generally decreases northward in the model domain, suggesting that the offshore tsunami hazard is greater for the southern part of the study area. For an ARI 10 000 year tsunami (exceedance rate calculated across all source zones), the spatial deaggregation was generally dominated by the Tonga-Kermadec and Puysegur source zones. However, the contributions from New Hebrides, South America and Outer-rise Puysegur zones were also noteworthy. Minor contributions from Outer-rise Tonga-Kermadec, Sunda and/or Mexico source zones were also identified.

It is important to recognise the uncertainties in recurrence interval calculations for large tsunamis. The maximum stage/ARI relationship in the PTHA is based on the mean values (as per the graph in Figure 3), so both larger and smaller maximum stage values occur within the 95% confidence interval for a given ARI. The wide range of values across this interval reflects the uncertainties around calculating frequencies of these large, rare earthquake events. By using the mean value we are effectively averaging over the uncertainties. The level of uncertainty in the source earthquake scenario is quantified in the PTHA by the 'weight with non-zero rate' parameter, which gives the fraction of weighted magnitude frequency curves that consider the scenario to be possible (ranging from 0 = impossible in all models, to 1 = possible in all models). The value of this parameter is determined from the subduction zone geometry and maximum possible earthquake magnitude on that segment. For example, a Mw 9.6 earthquake is considered to be the maximum possible magnitude on the Tonga-Kermadec Trench, but the Puysegur Trench is thought to only be capable of generating a Mw 8.7 earthquake. At an ARI of 10 000 years and beyond, it is typical to find a significant fraction of the PTHA logic-tree branches calculate the event to be impossible, which explains why this is an appropriate benchmark for a "reasonable worst case" scenario.

Three source zones were chosen for further exploration and modelling: Puysegur Trench, New Hebrides Trench and Tonga-Kermadec Trench (Figure 2). These sources were chosen because of their consistently high contributions to the aggregated mean rates at most PTHA hazard points along the 100 m depth contour. Despite the significant contribution of the South America source zone to the hazard deaggregation for the central study area, we chose not to perform inundation modelling for South America scenarios. Instead, we focus on those sources with shorter travel times to reach Tasmanian shores. The long travel times for far-field tsunamis, combined with the efficacy of tsunami monitoring programmes in the Pacific Ocean, allow for sufficient warning time for planning and evacuation. In addition, global-scale propagation models are usually run on a relatively coarse mesh and factors such as dispersion and friction may be ignored, which introduces extra complications for performing inundation modelling of far-field tsunamis.

In the case of the Puysegur and New Hebrides trenches, "outer rise" scenarios were also considered. Outer rise scenarios refer to tsunamis that are generated by earthquakes near, but not on, the respective subduction zone interface. In contrast to the reverse thrust earthquakes that occur on the subduction interface itself, the outer rise earthquakes included here are all normal fault sources. This distinction is important because the geometry of the tsunamigenic fault and its orientation with respect to the Tasmanian coastline determines whether the tsunami will arrive as a leading elevation wave (initial rise in water level) or a leading depression wave (initial drawback of water).

A total of 20 model scenarios were run, from the aforementioned tsunami source zones. The scenarios are summarised in Table 1 and their associated Scenario IDs are used in the following sections to describe the results. The scenarios were selected using the methods described in Geoscience Australia (2018), with the central hazard point used to define the return interval and maximum stage values for scenario selection.

The results from all 20 scenarios were compared across the region and four scenarios with approximately equal ARIs were designated for detailed analysis and comparison. These scenarios were chosen to represent the three primary subduction source zones (Puysegur, Tonga-Kermadec and New Hebrides), with the addition of an outer-rise scenario for Puysegur, given its significance as the nearest source zone to Tasmania.

TABLE 1: List of scenarios modelled in this study, summarised by source zone. The scenario ID relates to the source zone in question, plus the identification number assigned to each scenario in the PTHA 2018 database.

Source zone	Scenario ID	Mw	Max stage recurrence interval at hazard point
Puysegur	PU3514	8.7	8200
	PU3574	8.7	9100
	PU3679	8.7	11 600
	PU3509	8.7	11 800
	PU3506	8.7	13 400
	PU3531	8.7	39 000
Outer-rise Puysegur	OP3108	8.7	10 500
	OP3261	8.7	10 800
New Hebrides	NH12825	9.2	8800
	NH12551	9.1	9100
	NH12759	9.2	11 700
	NH12584	9.1	16 000
Outer-rise New Hebrides	ONH8056	8.9	10 400
Tonga-Kermadec	TK44046	9.5	8100
	TK43665	9.4	10 300
	TK43919	9.5	10 700
	TK43837	9.5	11 000
	TK43427	9.4	11 300
	TK43819	9.5	15 000
	TK43725	9.4	31 400

Designated scenarios are highlighted in red

Input data and model implementation

Boundary conditions

Time series data of the incoming tsunami water level and momentum for each of the 20 scenarios were obtained for 16 PTHA hazard points along the eastern model domain boundary. The files obtained from the PTHA database were in NetCDF format, which required conversion to ANUGA's proprietary *sts* format prior to use. The points approximately follow the 100 m depth contour (Figure 1), and any points located at < 90 m depth were excluded. The boundary condition time series cover a 36 hour period, which extends beyond the modelled timeframe. The top and bottom ocean segments of the boundary were transmissive, allowing the tsunami waves to exit the model domain without reflection.

Model resolution and mesh structure

The model was run on a variable resolution triangular mesh, with a total of 3 035 165 mesh elements. The unstructured mesh allows for flexibility in resolution and localised variations in areas of urban settlement or coastal complexity, while optimising computational memory and run time. The mesh resolution varied from coarse to extra fine (Figure 5, Table 2). Offshore areas and land > 15 m AHD were modelled on a coarse mesh (triangle length, dx, 400 m), whereas ocean areas between 30 and 10 m depth were modelled on a medium mesh (dx 200 m). Land areas were generally modelled at fine (dx 50 m) or very fine (dx 20 m) resolution, with these differing resolutions applied to rural and urban areas, respectively. Bicheno and St Helens were identified as areas of particular interest and/or complexity and were modelled at extra fine resolution (dx 10 m).

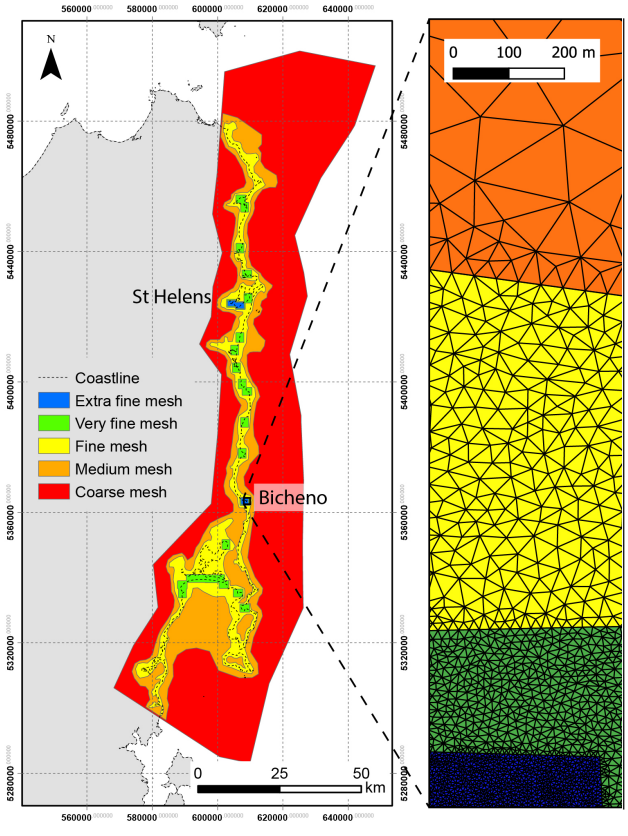

FIGURE 5: Details of mesh resolution zones across the study area.

TABLE 2: Mesh resolution zones and areas covered.

Mesh resolution	Triangle area (m^2)	Triangle length dx (m)	Coverage
Coarse	80 000	400	Open ocean and land > 15 m ASL
Medium	20 000	200	Offshore areas -30 > -10 m ASL
Fine	1250	50	Rural areas -10 m > 10 m ASL
Very fine	200	20	Urban areas of interest
Extra fine	50	10	St Helens, Bicheno

Elevation model

A 10 m composite Digital Elevation Model (DEM) was constructed by combining various topographic and bathymetric datasets (Table 3). The DEM is a bare earth model, excluding buildings, vegetation, and structures such as bridges. Buildings and vegetation were accounted for in the model through the Manning's *n* surface roughness parameter, as described in the following section.

The DEM was built in ArcGIS. Data was initially cleaned and assigned a hierarchy so that overlapping data could be removed. The DEM was then constructed in tiles, before the rasters were mosaicked into a single DEM covering the entire model domain. The terrestrial DEM processing is further detailed in Kain and Mazengarb (2020). Where LiDAR data was available, an elevation model for each survey was constructed from the point clouds using a mean binning technique to assign the elevation for each cell. In areas with no LiDAR coverage the DEM was constructed using a spline based interpolation method, from 10 m photogrammetric contours that were supplemented with spot height data.

The bathymetric model was constructed from navigational charts and nearshore bathymetric survey data (Table 3), and proved challenging in areas of sparse data coverage. To generate a 10 m model in the deep ocean areas (~50 m depth) using the available data, a model was first built at 200 m resolution and then oversampled to 10 m cell size before appending to the nearshore data. This should have little effect on the modelling, as the mesh resolution in these areas is very coarse (dx 400 m).

Areas of complex nearshore bathymetry were manually inpected to ensure they were accurately represented in the DEM, as poor elevation control can have significant implications for the quality of the model outputs. The St Helens bar and channel was one area that was poorly captured by the spline interpolation algorithm. This issue was rectified by manually adding a relatively dense array of additional elevation points along the channels and intertidal areas and re-running the interpolation.

The elevations assigned to the manual points were based on the AusENC navigation charts and the map published by Mount et al. (2005). Additional points were added along the length of the channel, but particular care was taken to accurately represent the St Helens Barway and St Helens Important Bird Area (IBA), as these shallow sandy features would interact considerably with any incoming tsunami wave (Figure 6). It is important to note that the sandy channel area is a mobile landform, and a comparison of historic aerial imagery shows some geomorphological variation over time that is not accounted for in the modelling.

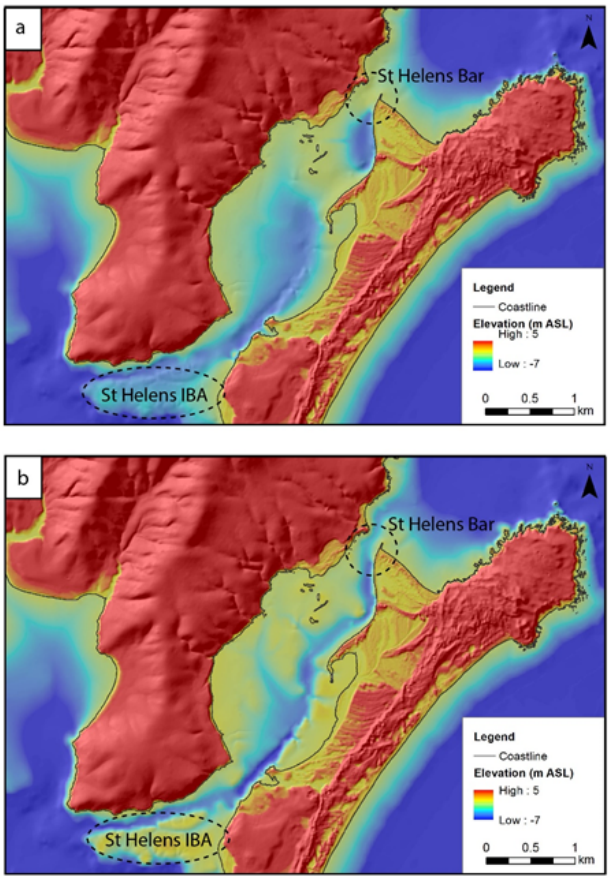

FIGURE 6: Comparison of the initial and modified DEMs for the St Helens channel area.

a) Automatically generated DEM interpolated from the known data points.
b) Interpolated DEM after the addition of manual points and low-water-mark contours.

TABLE 3: Data sources used to construct the elevation model.

Data source	Type	Year	Source
Terrestrial LiDAR surveys	LAS point cloud	2008-2019	Geoscience Australia, National Elevation Data Framework (NEDF/ELVIS)
TAS DEM 25m	Photogrammetric (topographic) contours		DPIPWE (2007)
SeaMap Tasmania	5 m contours (bathymetry)	up to 2007	Lucieer (2007)
Mean High Water Mean Low Water	Contours	2015	DPIPWE (2015)
AusENC (Australian Hydrographic Office)	Depth soundings (bathymetry)	up to 2018	Licenced data
Australian Bathymetry and Topography Grid	National gridded bathymetry model (200 m resolution)	2009	Whiteway (2009)

Manning's *n* surface roughness model

Tsunami wave attenuation and flow patterns are strongly influenced by surface roughness and land cover. Seafloor surface type will influence the attenuation of the tsunami waves offshore, whereas the presence and type of vegetation cover, buildings and coastal waterbodies will affect tsunami run-up distances and flow patterns onshore.

A surface cover map of the model domain was created in ArcGIS, at a spatial resolution of 10 m (Figure 7). The surface map was generated from statewide datasets, including the LIST Tasmania road layer (Land Information System Tasmania, 2019). Vegetated areas were mapped using the TASVEG layer (DPIPWE, 2013), and LiDAR data was used to define building footprints, which were stamped over the other data as a final step.

Variations in surface cover were applied in the model using the Manning's *n* parameter, with Manning's *n* coefficients assigned by surface type (Table 4). Appropriate values for each surface type were selected based on the Australian Rainfall and Runoff Guidelines (Ball et al., 2019).

TABLE 4: Manning's *n* coefficients of roughness applied in the model, as assigned by surface type.

Manning's *n*	Surface Type
0.5	Solid buildings
0.071	Built-up areas
0.055	Vegetated areas
0.035	Land (default)
0.03	Bare ground
0.025	Water courses
0.018	Roads
0.01	Oceans and estuaries

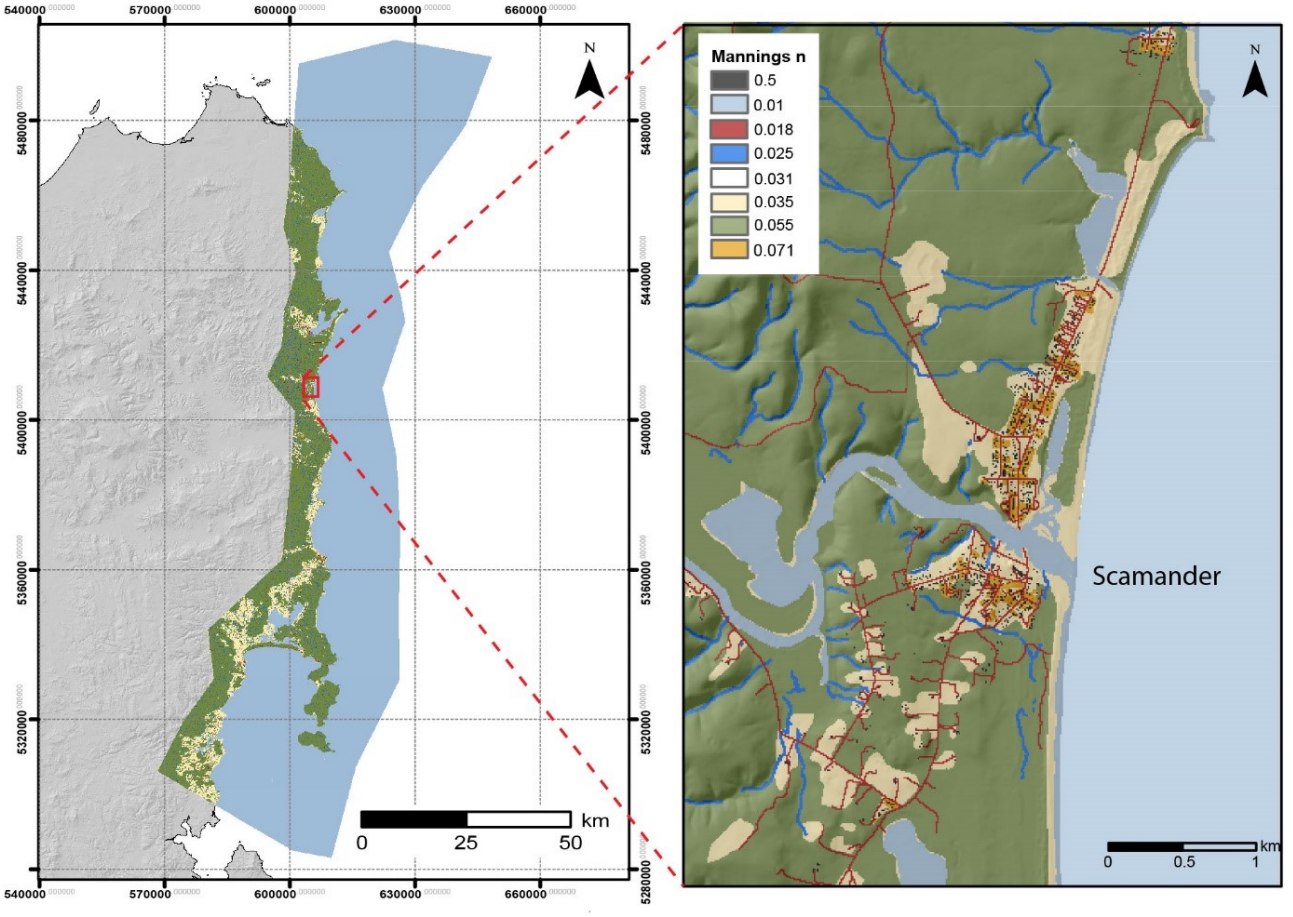

FIGURE 7: Manning's *n* zones as applied across the model domain, with a detailed example of the Scamander area.

Dune erosion zones

Sand bars and dune systems can have a significant effect on tsunami inundation patterns. Such systems may initially afford some protection to land and communities behind, but they may be eroded by the first wave and leave the surrounding area more exposed to inundation from subsequent waves in the tsunami wave train.

There are several locations where large sand bars and dune systems were accounted for in the model, including Ansons Bay, St Helens, Scamander and Dolphin Sands (Figure 8). Dune erosion for these areas (as defined by the polygon shapefile provided in Appendix 7) was incorporated into the model using the operator script developed for the south east Tasmania tsunami modelling project (Rigby et al., 2017). This erosion operator is based on the methods of Froelich (2002) and simulates the erosion process but not subsequent sediment transport and deposition.

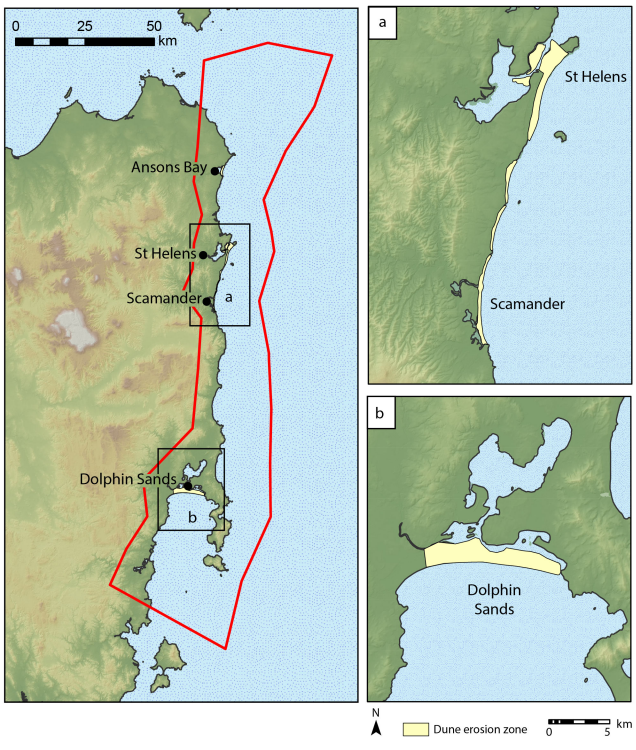

FIGURE 8: Locations of the areas modelled with the active dune erosion operator.

Simulation using ANUGA

The tsunami simulations were performed using ANUGA, which is a free and open source hydrodynamic modelling library developed by Geoscience Australia and the Australian National University (Nielsen et al., 2005; Roberts et al., 2019). Since its release in 2006, ANUGA has been widely used to simulate tsunami inundation and several studies have compared ANUGA-derived results with historical events (e.g. Jakeman et al., 2010) or other modelling packages (Fernandes 2009; Mungkasi and Roberts, 2013) and found the results aligned well.

ANUGA uses a finite volume solution to resolve the two-dimensional shallow water wave equation, and the DE0 flow algorithm was used in this study. The tsunami modelling scripts were built in Python 2.7 and the processing was performed on a remote access server running Ubuntu version 18.05 with 256 Gb of RAM.

As the objective was to examine a worst case scenario of tidal-tsunami interaction, the initial water level was set to Highest Astronomical Tide (HAT). The use of HAT is likely to give a more conservative (greater) tsunami inundation estimate than mean sea level (MSL), as was shown in south east Tasmania when comparing model runs at HAT with the same scenario run at MSL and LAT. However, other tsunami parameters such as velocity and wave steepness may be more extreme at lower water levels. An approximate HAT value of 0.8 m AHD was applied across the entire model domain, which represents an average value for eastern Tasmania (range 0.7-0.86 m AHD). The models were not run with a dynamic tide, as this would add considerably to the already heavy computation time. In addition to a significant increase in simulation time, extra model runs would then need to be completed for each scenario to examine the sensitivity of each to tidal phase. This process was not considered to be feasible for such a large model.

Data processing

Raster and time series data of water level and velocity were extracted from the NetCDF model files and analysed in a GIS environment. Maximum flow depths (onshore) and maximum velocities (offshore) were mapped and tsunami wave time series were generated at 65 locations (Figure 9).

Model validation and sensitivity testing

The model was validated against the results for the previous modelling in south east Tasmania by comparing the model results from similar Puysegur scenarios to those of the south east modelling. The bottom quarter of the model domain was set to overlap with the south east model domain, so simulated flooding extents, flow depths and velocities could be directly compared. The results were found to agree well in areas where the mesh resolution was the same between the two models. In cases where the south east mesh was coarser, or bathymetry was poorer, the south east model results showed greater run-up and inundation.

The sensitivity of the model with respect to the underlying elevation data and mesh resolution was tested around the St Helens area, where the coastline contains both complex and more linear elements. The model was first run on a largely unmodified St Helens dataset, with a fine (dx 50 m) to very fine (dx 20 m) mesh in the nearshore zone and dune erosion enabled in the channel area. The bathymetry was progressively modified in the channel and re-modelled, and finally the mesh refined to extra-fine (dx 10 m) in the entire Georges Bay area. Results were compared for these model runs and the differences in maximum tsunami amplitude were found to be between 0.03 m (time series gauge 56) and 0.67 m (gauge 53) around the bar, channel and IBA. The largest differences were observed immediately inside the St Helens barway. Without proper representation of the channel, the bar was acting as a barrier, causing the tsunami waves to be erroneously attenuated. There was very little variation in inundation extent at St Helens, although the less detailed model was slightly more conservative (i.e. the flooding footprint was marginally greater).

The sensitivity to Manning's *n* values was not explored in this model. The values were taken directly from the south east Tasmania tsunami modelling study, where they had been tested and refined as part of the model development process.

FIGURE 9: **Time series point locations. Numbers correspond to file names in Appendix 4.**

RESULTS

General overview

This section provides a summary of the results across all modelled tsunamis, but the location-specific results focus primarily on the four designated scenarios. We recommend readers refer directly to the maps and spatial data supplied in Appendices 3 and 4 if they are interested in the details of the supplementary scenarios. It is also important to note that this study is intended to explore the impacts of a "maximum credible" tsunami and does not consider the impacts of smaller, more frequent, tsunamis. Although some specific impacts are described, these are not exhaustive and results do not constitute a tsunami risk assessment.

For all modelled subduction-interface tsunamis, the first wave arrived as a leading elevation N-wave, which manifests as an initial rise in water level. However, the outer rise tsunamis from both Puysegur and New Hebrides trenches arrived as leading depression waves. The leading depression waves would result in the sea receding dramatically at the shoreline before the arrival of the first wave peak. For all scenarios, significant waves arrive at the coast periodically over the 12 hours following the first wave. In most cases the first or second waves were the largest, although in isolated cases later arriving waves were comparable in size to the first or second wave.

Tsunami arrival times for each source zone were consistent along the open coast, with only a 6 minute delay between the south and north of the study area for Puysegur scenarios, and no difference for Tonga-Kermadec or New Hebrides sources. Travel times for Puysegur scenarios were approximately 2 hours 10 minutes, whereas Tonga-Kermadec and New Hebrides tsunamis were 5 hours 25 minutes and 5 hours 10 minutes, respectively. Tsunami travel times for key locations are summarised in Table 5.

As the tsunami waves approach shore and the water depth becomes shallower, wave height increases and both velocity and wavelength decrease. Tsunami wave periods were 25-30 minutes for all scenarios, calculated offshore to avoid any influence of reflected waves near the coast. Although this is the period for the main tsunami waves, water levels would likely rise and fall more frequently near the coast, due to bathymetric influence, wave interference and reflection from coastal landforms.

Simulated tsunami inundation was greatest in east-facing open coast areas, which were directly exposed to incoming tsunami waves. Maximum tsunami wave amplitude reached > 7 m along the open coast in the south, but only reached 5 m in the north of the model domain. Onshore run-up height consistently reached 7 m AMSL. In many areas, modelled run-up was tightly controlled by the topography and so inundation footprints were similar for all scenarios. However, simulated flow depths were generally greater for larger tsunamis. The most affected townships include Scamander and Douglas River, with St Helens, Beaumaris and Bicheno also experiencing some impact. Many settlements are situated > 8 m AMSL and were unaffected in the simulations, beyond some inundation of beaches and low-lying reserve areas nearby. The A3 Tasman Highway extends along the length of the model domain and results indicate that it would be flooded or washed out at several locations, particularly in the south of the study area where it follows the coast along low-lying plains.

TABLE 5: Summary of tsunami travel times by source zone, for key locations in the study area.

Source zone	Location	Tsunami travel time
Puysegur Trench	Bicheno	2 h 10 m
	Scamander	2 h 16 m
	St Helens	2 h 40 m
	Ansons Bay	2 h 17 m
New Hebrides Trench	Bicheno	5 h 19 m
	Scamander	5 h 11 m
	St Helens	5 h 40 m
	Ansons Bay	5 h 10 m
Tonga-Kermadec Trench	Bicheno	5 h 24 m/ 5 h 50 m
	Scamander	5 h 27 m/5 h 52 m
	St Helens	5 h 50 m/ 6 h 13 m
	Ansons Bay	5 h 26 m/ 5 h 52 m

Note that two sets of travel times are given for the Tonga-Kermadec Trench. The first refers to tsunamis originating at the northern end of the trench and the second refers to the southern portion of the trench.

The results were consistent when comparing the outputs of all 20 scenarios. In areas with tightly constrained topography, the run-up did not change significantly across the scenarios, but flow depths were generally greater for larger tsunamis (e.g. Bicheno – Figure 10). In areas of flatter topography, inundation footprints and flow depths were more variable between scenarios (e.g. Lagoons Beach – Figure 11). Horizontal distance variations ranged from 20 m to > 200 m in extreme cases, particularly at the heads of inlets and lagoons.

Variability between scenarios was not solely dependent on topography, and a greater ARI alone (as calculated from the PTHA at the 100 m depth contour) did not directly predict larger incoming wave heights or greater inundation. In some places, inundation limits were specific to site orientation with respect to source zone. For example, in east-f acing bays Outer New Hebrides 8056 (ARI = 10 400 years) usually travelled farther inland than all other scenarios, including Puysegur 3531 (ARI = 39 000 years) and Tonga-Kermadec 43725 (ARI = 31 400 years). Moreover, in many locations the inundation limit for the extreme Puysegur 3531 scenario (ARI = 39 000 years) was exceeded by several tsunamis with ARIs ≤ 13 000 years.

Detailed scenario footprints are provided in the multi-scenario map series (Appendix 3). These comparisons are explored further in the Discussion section of this report. Additional region-specific results for the four designated scenarios are described in the following sub-sections.

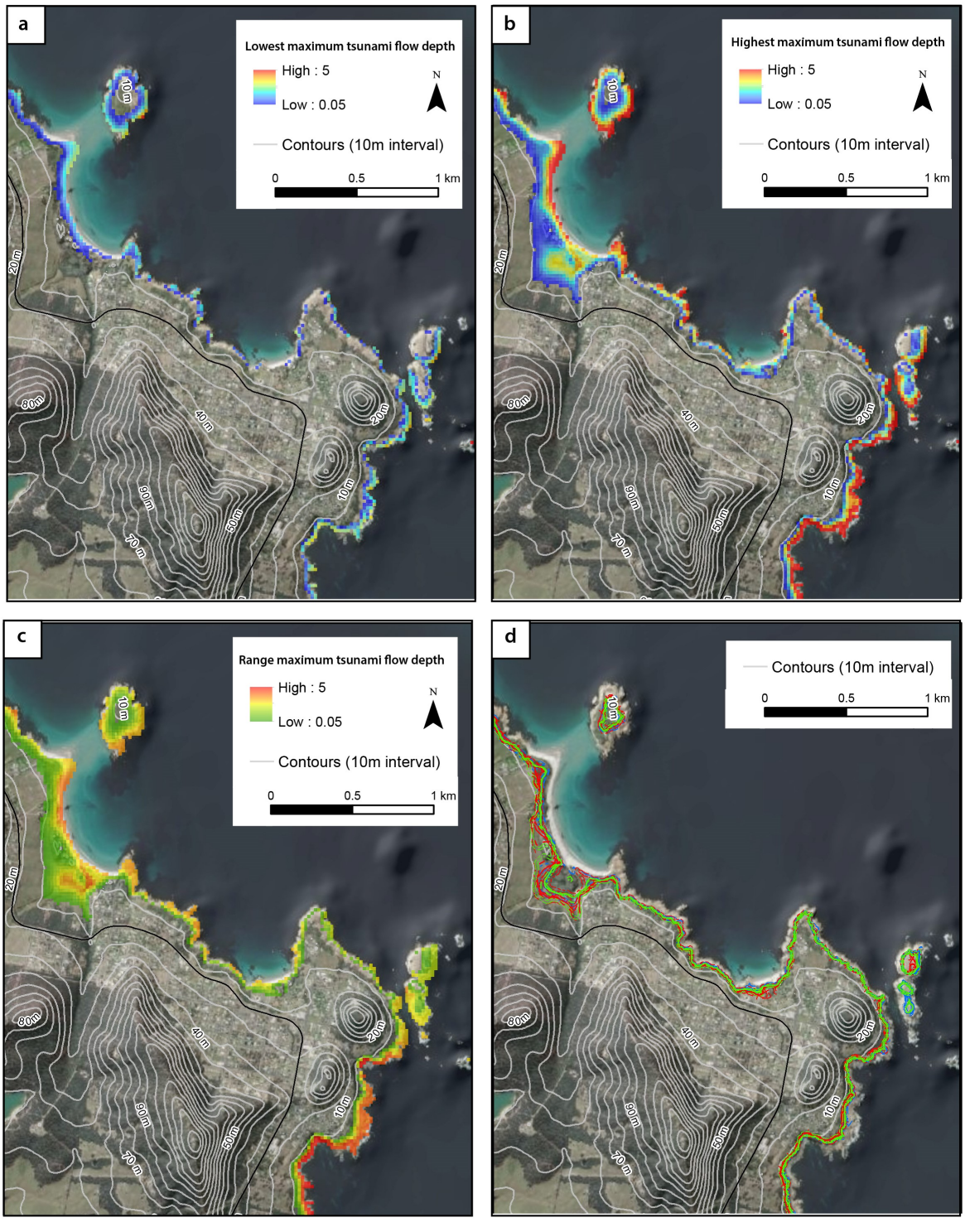

FIGURE 10: **Variability between tsunami scenarios at Bicheno, showing the aggregated range of tsunami flow depths across all 20 scenarios. a) Lowest maximum tsunami flow depth. Note that the values for each cell may not be from the same scenario. b) Highest maximum tsunami flow depth. Note that the values for each cell may not be from the same scenario. c) Range of maximum tsunami flow depths. d) Inundation footprints of all 20 scenarios. See Appendix 3 for a more detailed image.**

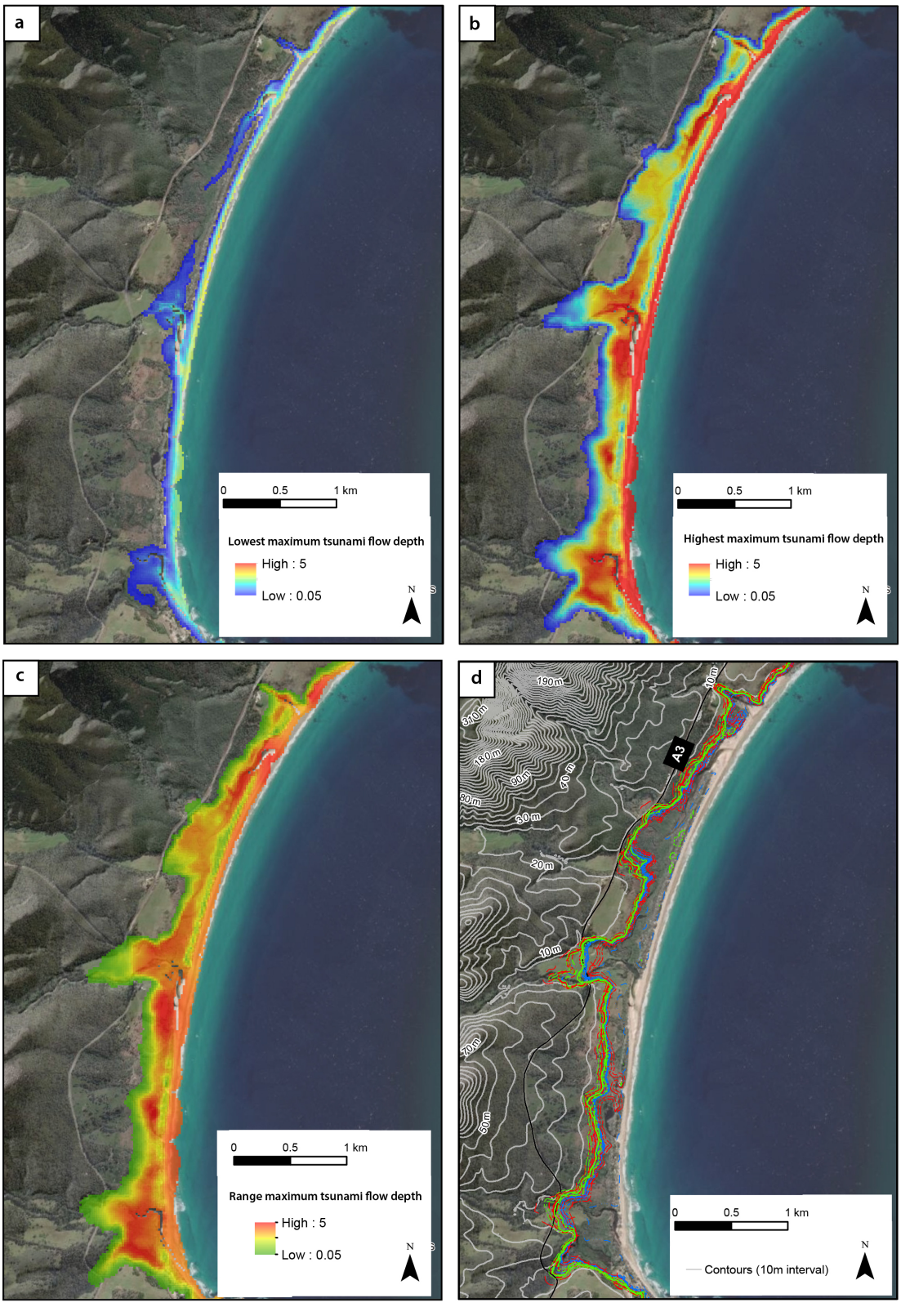

FIGURE 11: **Variability between tsunami scenarios at Lagoons Beach, showing the aggregated range of tsunami flow depths across all 20 scenarios. a) Lowest maximum tsunami flow depth. Note that the values for each cell may not be from the same scenario. b) Highest maximum tsunami flow depth. Note that the values for each cell may not be from the same scenario. c) Range of maximum tsunami flow depths. d) Inundation footprints of all 20 scenarios. See Appendix 3 for a more detailed image.**

Location-specific results

Swansea - Freycinet Peninsula - Bicheno (Maps 1-18)

The modelling results show the greatest tsunami inundation in this area occurs on the exposed ocean side of Freycinet Peninsula, with incoming wave amplitudes commonly around 7 m at Wineglass Bay. One or more waves in some scenarios show amplification due to the shape of the bay, resulting in maximum wave amplitudes of > 8 m (Figure 12). The inundation footprint at Wineglass Bay is largely controlled by topography, with the tsunami waves primarily travelling via Indigo Creek into the lagoon behind the beach (Figure 13). Run-up on the beach itself is tightly constrained by topography, but water levels reach 5 m AMSL on the beachfront.

Results show minor tsunami inundation for locations around Great Oyster Bay, such as Swansea and Coles Bay. The tsunami wave energy is significantly attenuated as it travels through the bay, resulting in maximum incoming wave amplitudes of 1.2-3.1 m and 2.5–3 m at these two locations, respectively. Tsunami inundation at Swansea is restricted to the esplanade and immediate beach areas. Some properties along Esplanade and Bridge Street are within the boundary of the inundation zone, but most of the township is outside the flooding footprint for all scenarios (Figure 14). Although the inundation is small for all scenarios, the Puysegur simulations produce greater wave heights and run-up elevations than the New Hebrides simulations.

Simulated tsunami inundation is relatively minor around Bicheno township for all scenarios (Figure 15). The maximum incoming wave amplitude is approximately 5.8 m, and tsunami run-up height on land reaches 7 m AMSL. Most of Bicheno is situated above 7 m AMSL and is outside the inundation footprint; however, properties closest to the coast may experience minor flooding. In addition, the lower lying areas north of the main township experience moderate flooding. Several sewerage pump stations and the Bicheno wastewater treatment plant are within the flooding footprint in these areas and the A3 Tasman Highway would likely be flooded behind the lagoon.

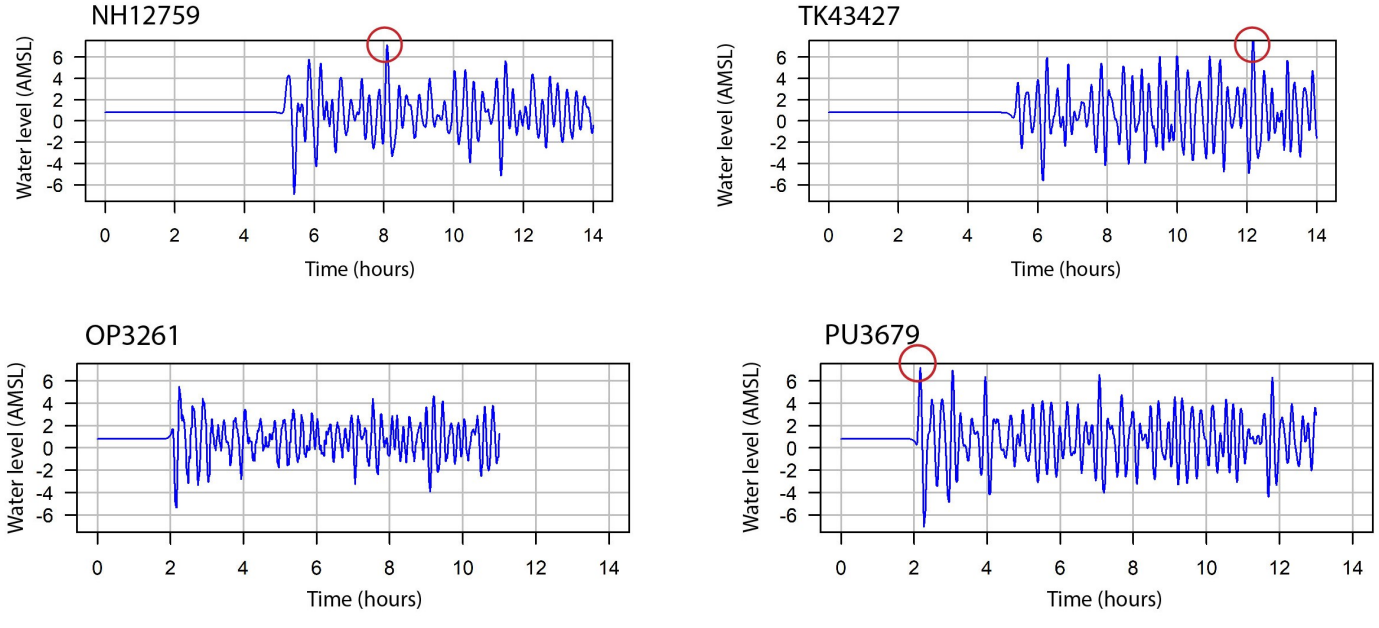

FIGURE 12: Simulated tsunami time series at Wineglass Bay for the four designated scenarios. Maximum amplitude is circled in red.

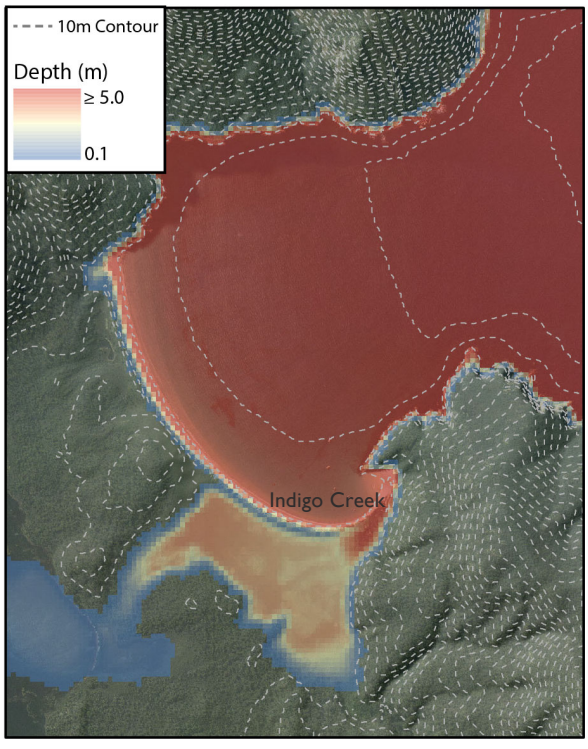

New Hebrides - NH12759

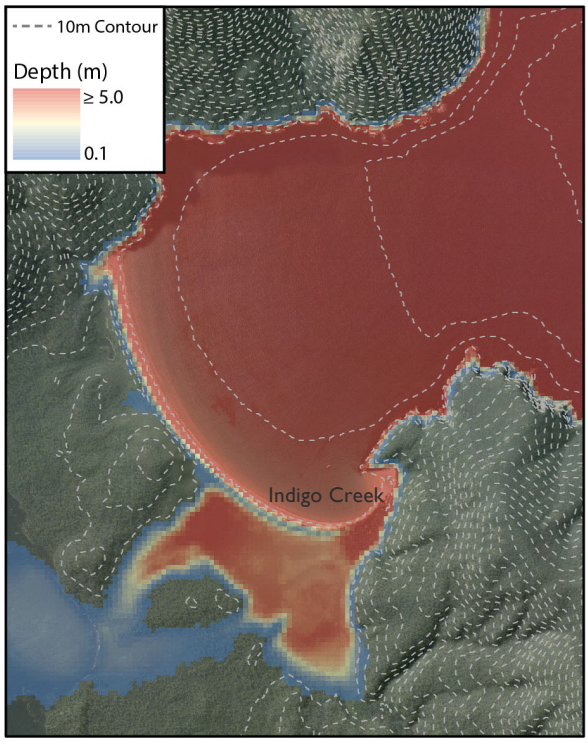

Tonga-Kermadec - TK43427

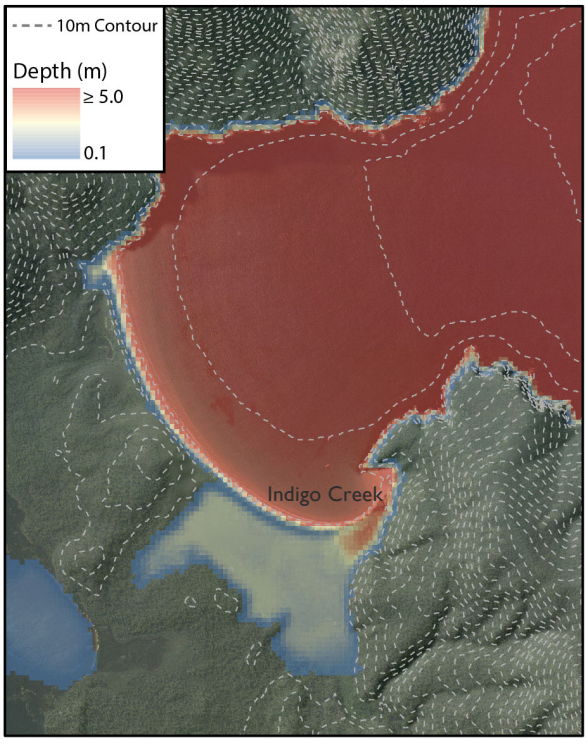

Outer Puysegur - OP3261

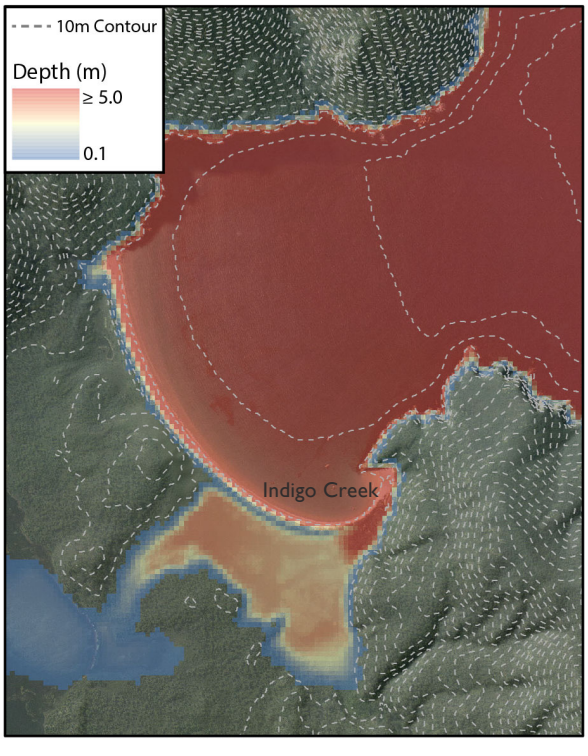

Puysegur - PU3679

FIGURE 13: Modelled tsunami inundation around Wineglass Bay for the four designated tsunami scenarios.

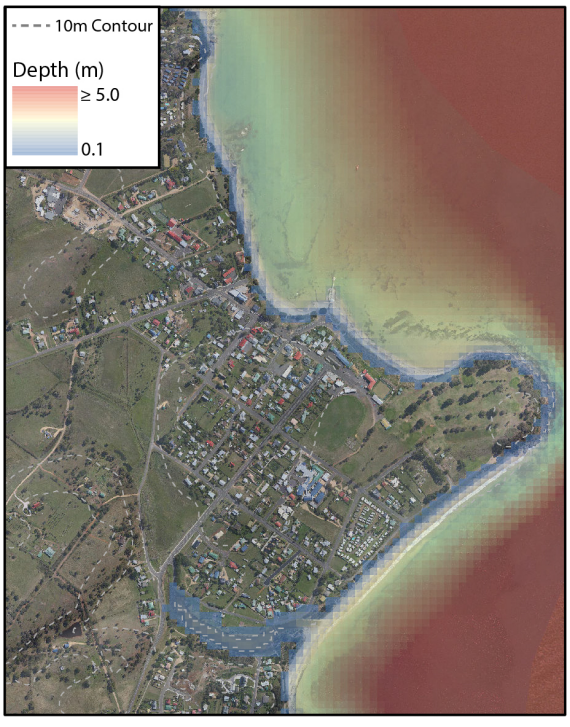

New Hebrides - NH12759

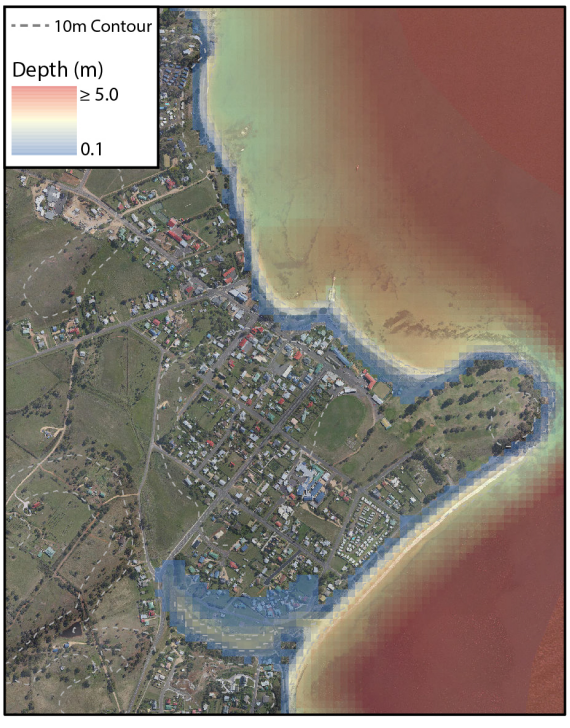

Tonga-Kermadec - TK43427

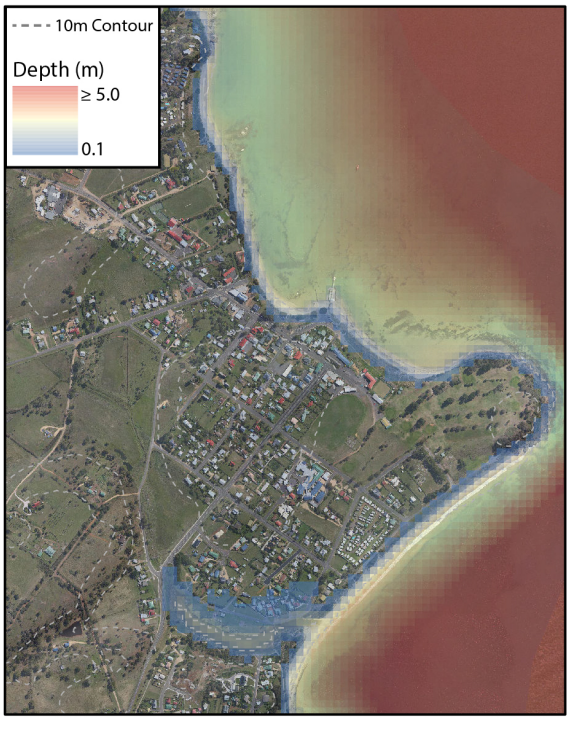

Outer Puysegur - OP3261

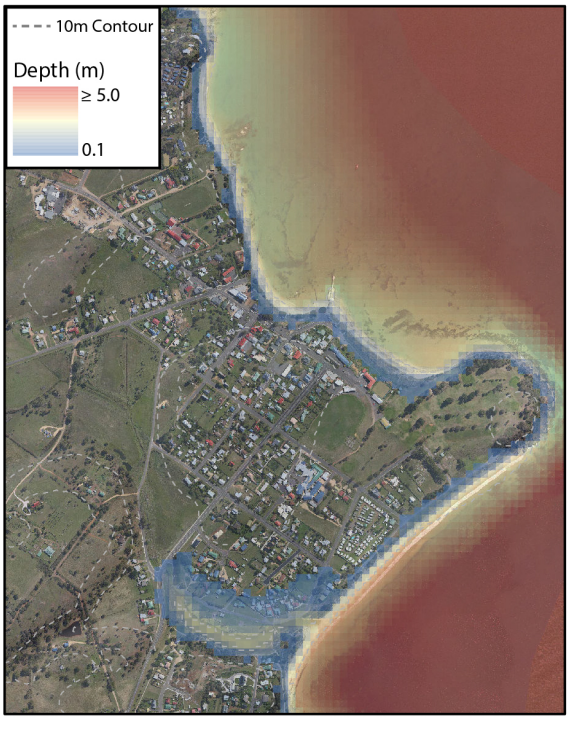

Puysegur - PU3679

FIGURE 14: Modelled tsunami inundation around Swansea, for the four designated tsunami scenarios.

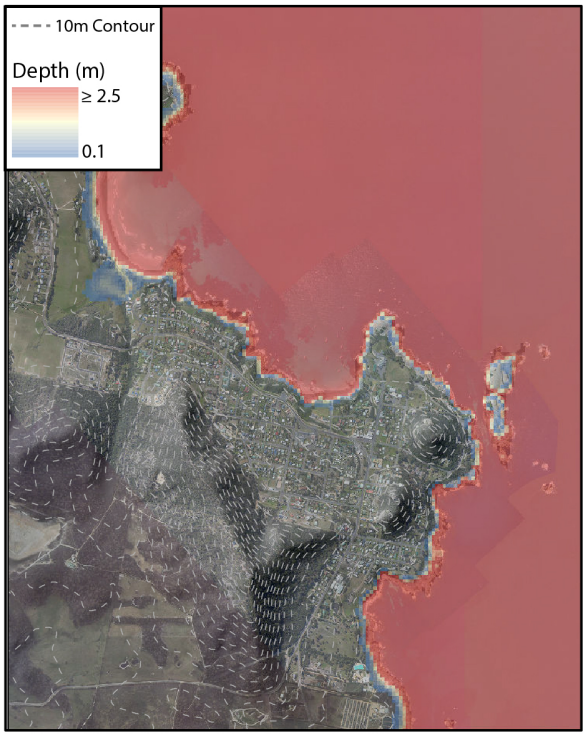

New Hebrides - NH12759

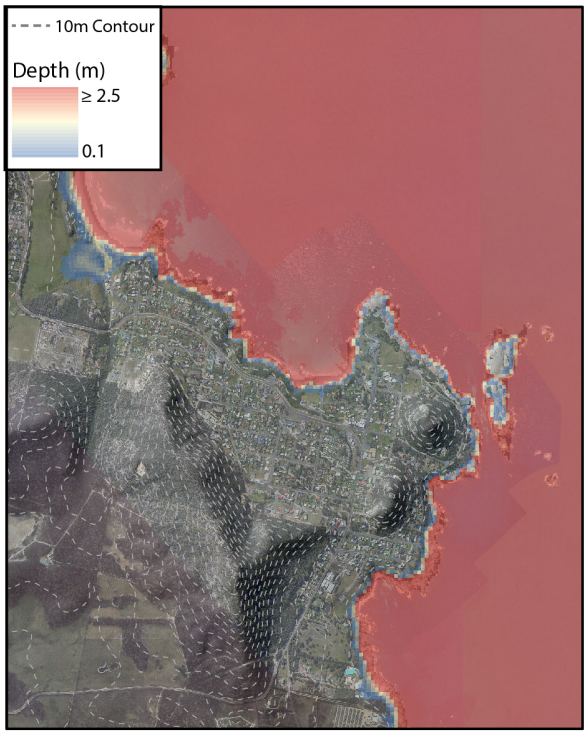

Tonga-Kermadec - TK43427

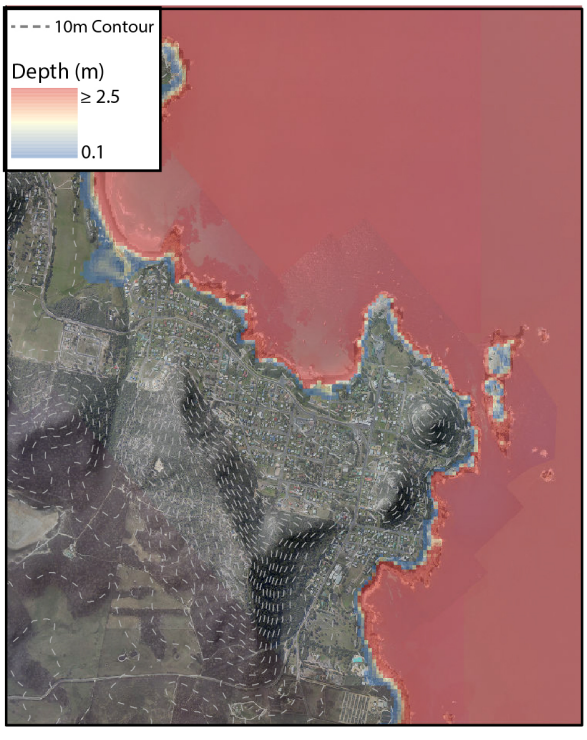

Outer Puysegur - OP3261

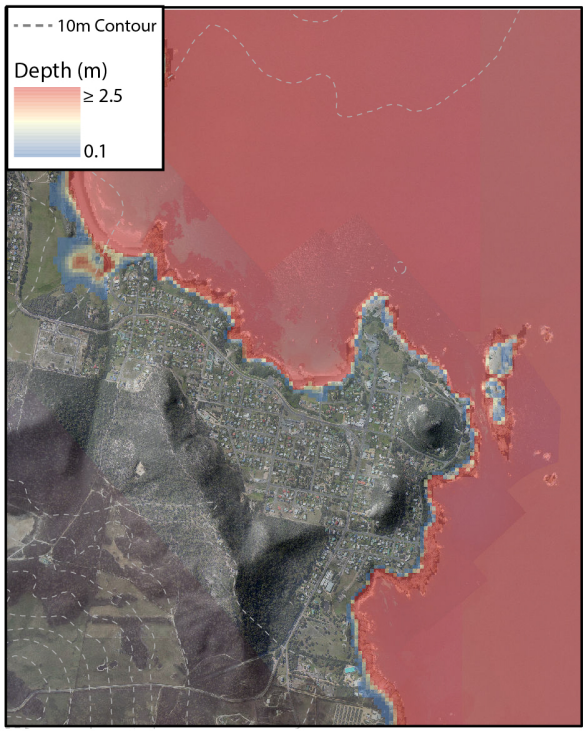

Puysegur - PU3679

FIGURE 15: Modelled tsunami inundation around Bicheno for the four designated tsunami scenarios.

Douglas River - Seymour - Lagoons Beach (Maps 19-23)

This stretch of coastline is characterised by long sandy beaches that are enclosed by rocky promontories and fed by river-mouth lagoon systems. Maximum incoming wave amplitudes reach 6 m (Figure 16) and model results show tsunami inundation that is primarily controlled by the geometry of the bays and promontories, with the lagoons and rivers acting as conduits for the tsunami flow inland.

Denison Rivulet and Douglas River are small rural communities where modelling results show flow depths of up to 2 m (Figure 17). A number of properties in the flooding footprint are tourist accommodation providers, including the campground at Douglas River. Results also show flow depths of up to 2.3 m across the A3 Tasman Highway at Denison Rivulet, with approximately 1 km of highway within the flooding footprint at this location.

Inundation around the Seymour promontory is limited as most of the promontory is situated above 10 m AMSL. Some inundation of land around Doctors Creek and Templestowe Lagoon can be seen, and a small number of dwellings and local access roads are within this area. North of the promontory, the Chain of Lagoons area is significantly affected and flow depths of 2-4 m occur at the Lagoons Beach campground.

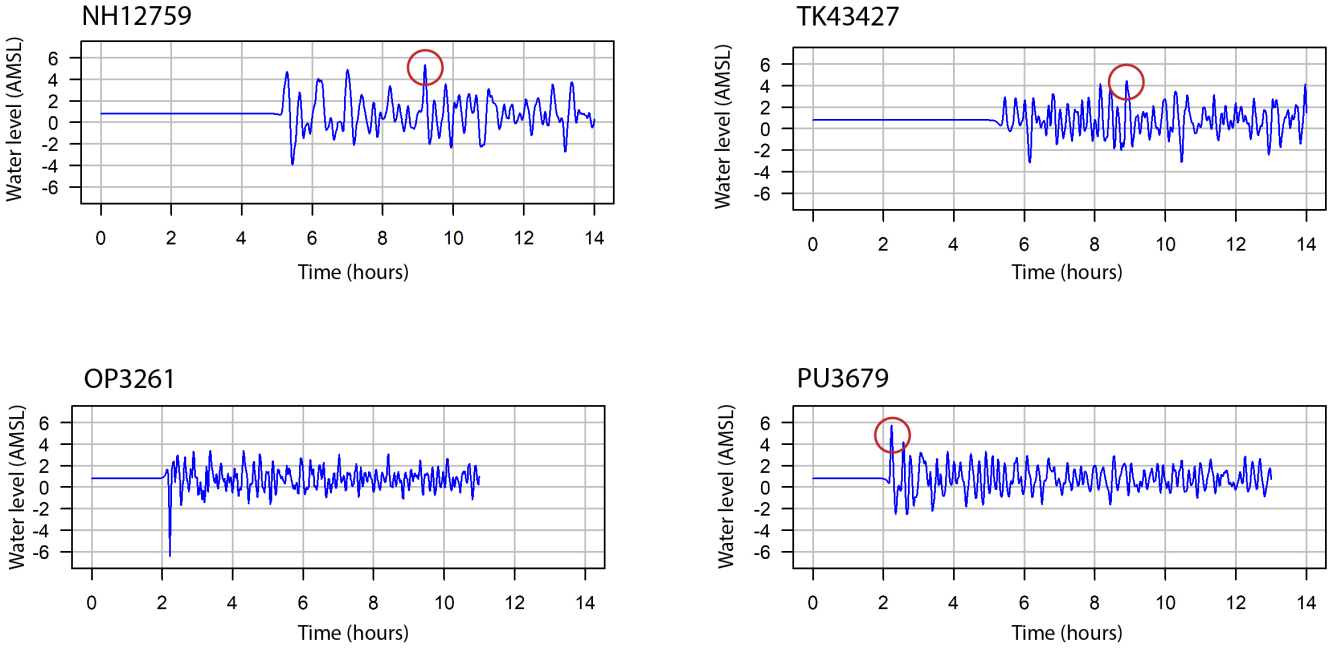

FIGURE 16: Simulated tsunami time series at Lagoons Beach. Maximum amplitude is circled in red.

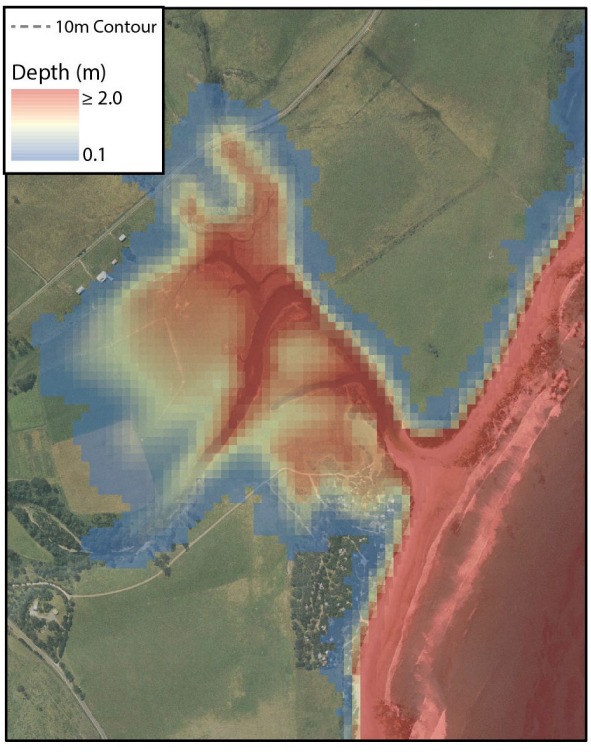

New Hebrides - NH12759

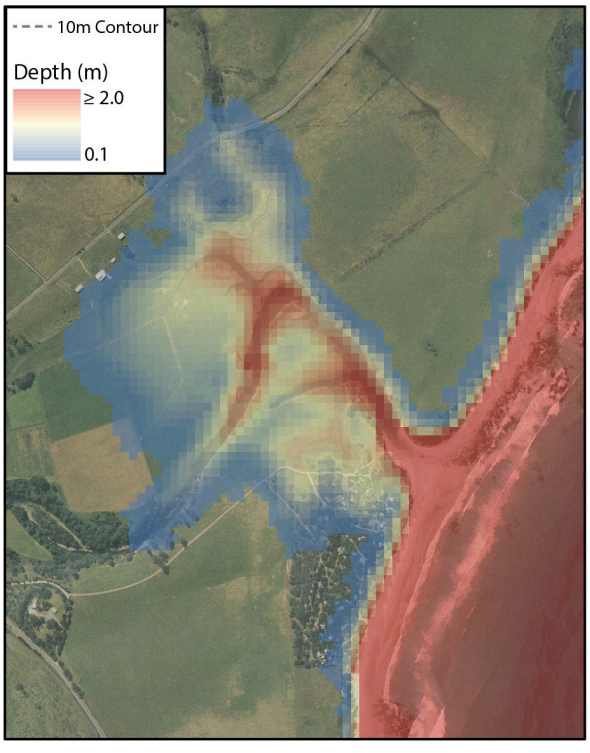

Tonga-Kermadec - TK43427

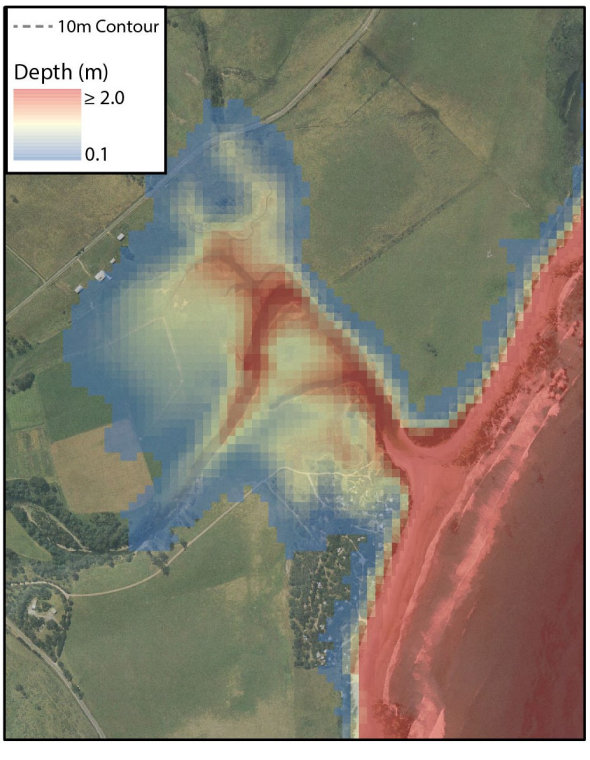

Outer Puysegur - OP3261

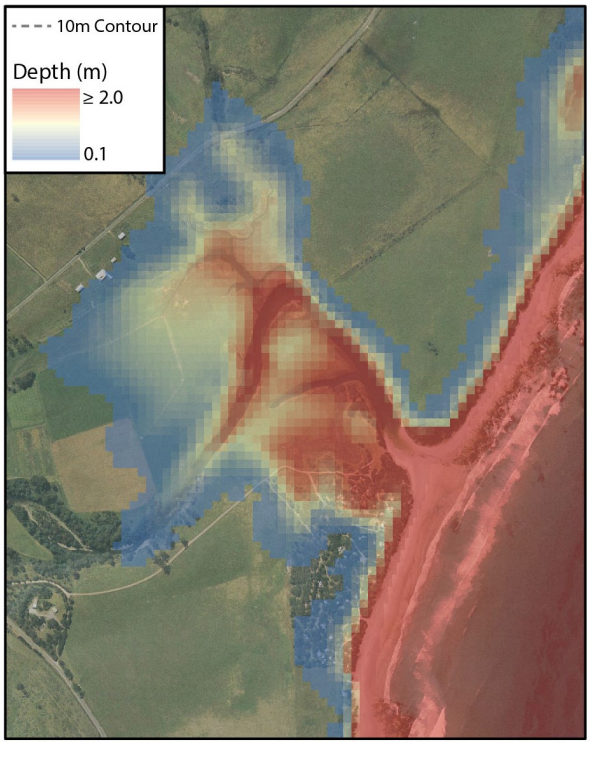

Puysegur - PU3679

FIGURE 17: Modelled tsunami inundation around Douglas River for the four designated tsunami scenarios.

Four Mile Creek - Falmouth - Scamander - Beaumaris (Maps 24-29)

The topography of this stretch of coastline is highly variable, with high rocky promontories interspersed with sandy lowland areas. Modelled tsunami inundation is noteworthy in these lower areas, with incoming tsunami wave amplitudes of up to 6 m, and onshore flow depths of up to 2.5 m. The inundation footprint is topographically controlled, with run-up height reaching 7 m AMSL.

The most significant impacts occur around the river mouth and lagoon at Scamander, although much of the township is situated above 7 m AMSL and beyond the limit of simulated tsunami inundation. The incoming tsunami wave amplitude is up to 6 m (Figure 18), with flow depths onshore of ≥ 3 m around the river and lagoon (Figure 19). A number of properties are situated within the inundation footprint, including residential areas and several cafes. In terms of infrastructure, the A3 Highway bridge across the Scamander River would likely be affected, along with several sewerage pump stations, sewerage mains and water mains (Figure 20). Erosion of sand around the Scamander river mouth and lagoon area would be significant, leading to infrastructure scour, changes in channel geometry and deposition of sediment on land. Significant current speeds would occur around the river mouth and lagoon area.

Most of the smallest townships on this stretch of coastline are located on high ground (> 10 m AMSL) and are outside of the tsunami run-up zone. However, limited inundation of beachfront properties at Four Mile Creek and Beaumaris can be seen. All dwellings at Falmouth appear to be situated above the tsunami run-up limit, but a large area of farmland to the west of the township is inundated with relatively shallow flow depths of < 1.2 m (Figure 21).

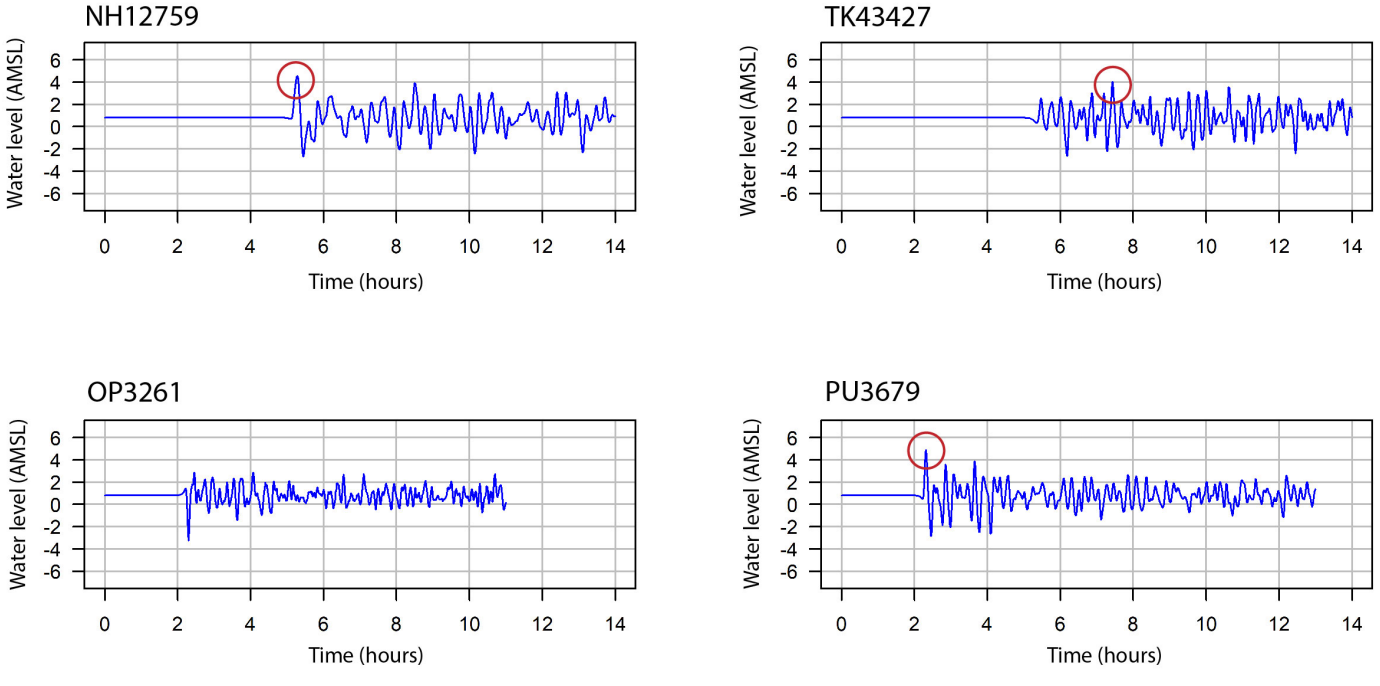

FIGURE 18: Simulated tsunami time series at Scamander. Maximum amplitude is circled in red.

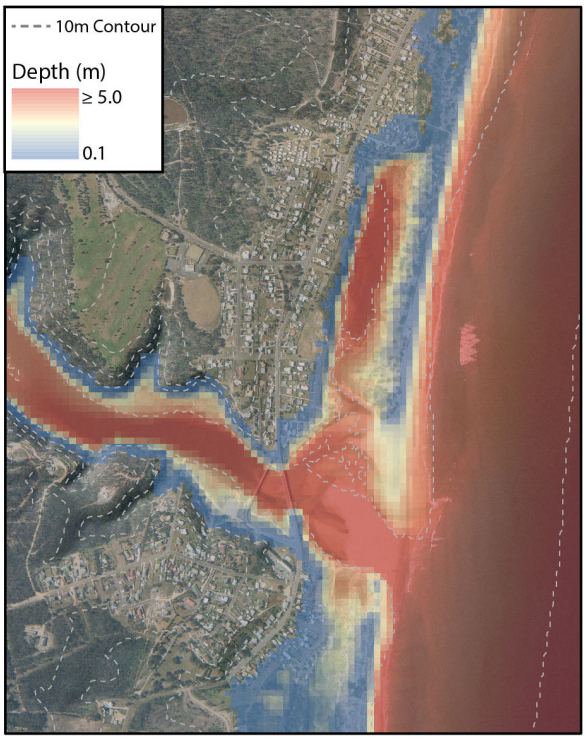

New Hebrides - NH12759

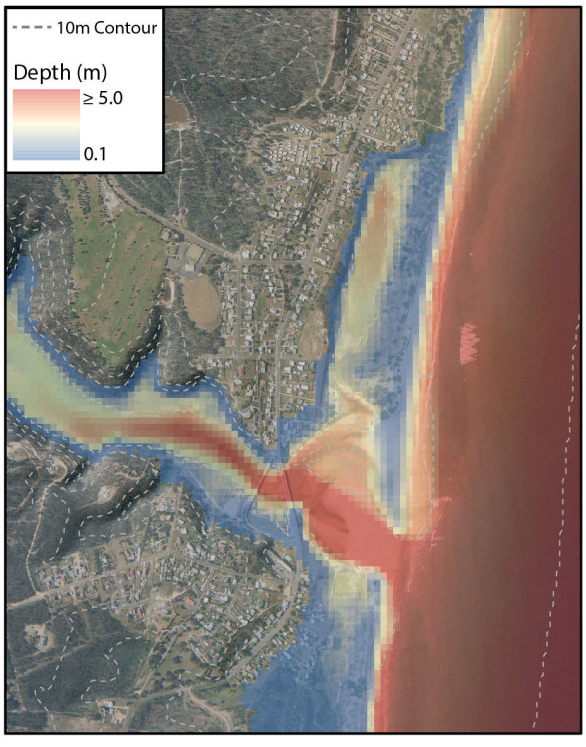

Tonga-Kermadec - TK43427

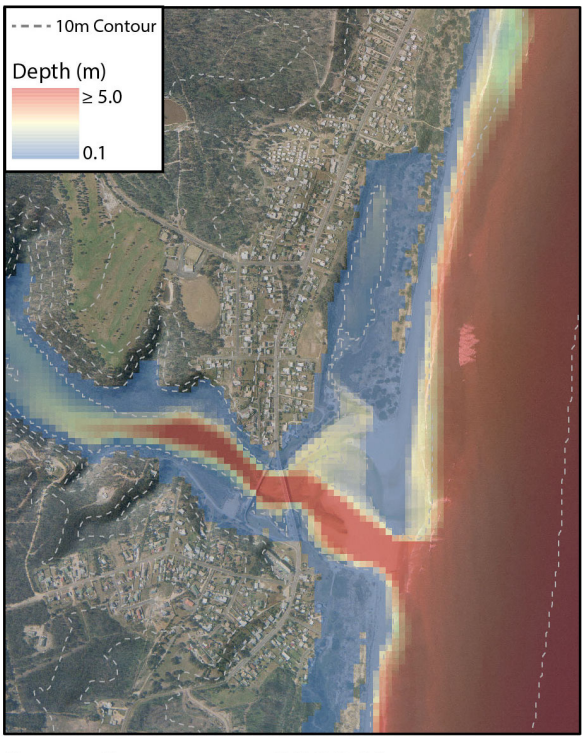

Outer Puysegur - OP3261

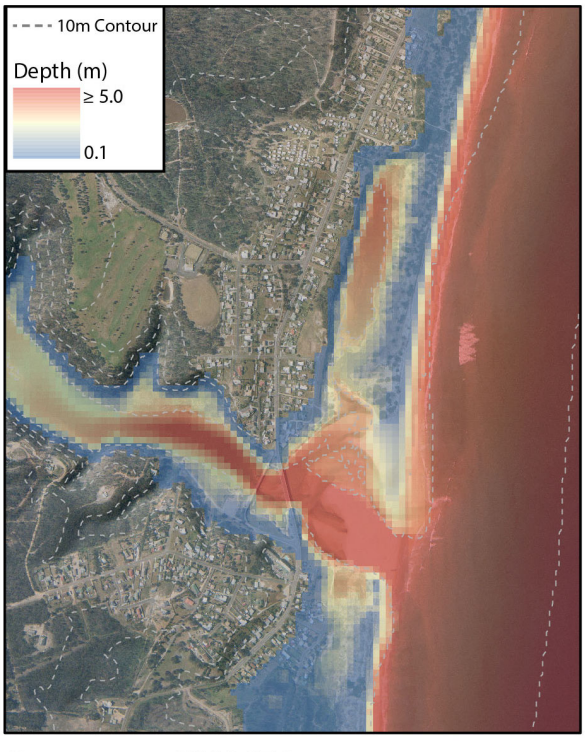

Puysegur - PU3679

FIGURE 19: Modelled tsunami inundation around Scamander for the four designated tsunami scenarios.

FIGURE 20: Map of infrastructure in the flooding zone at Scamander for PU3679. Data from ListData (2019).

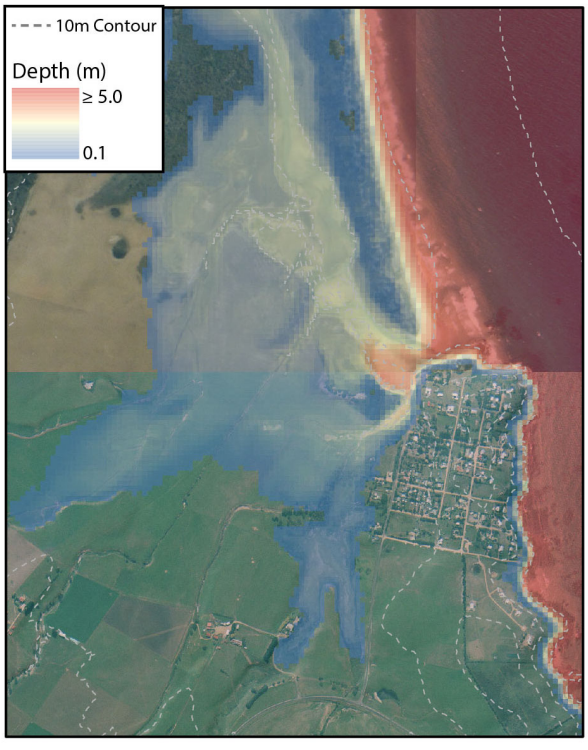

New Hebrides - NH12759

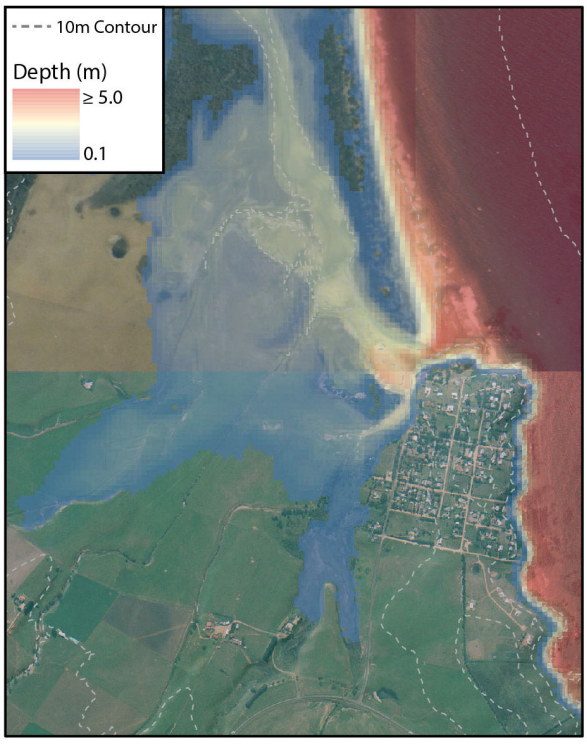

Tonga-Kermadec - TK43427

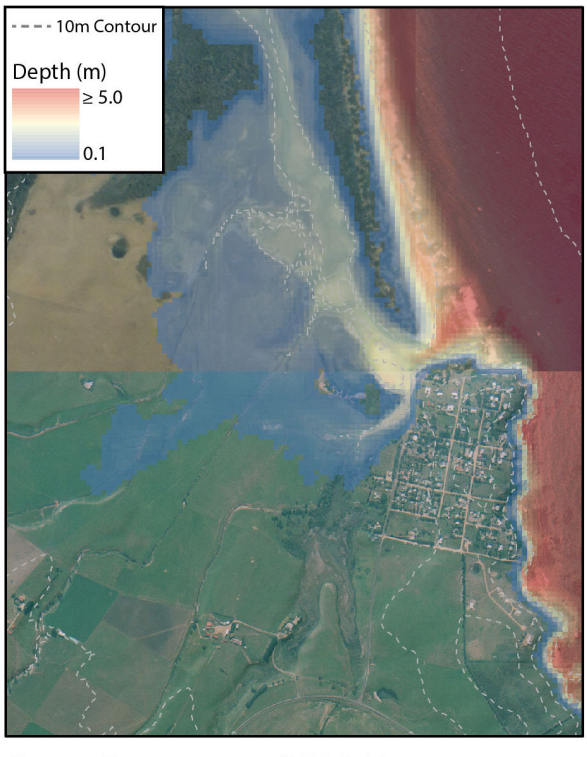

Outer Puysegur - OP3261

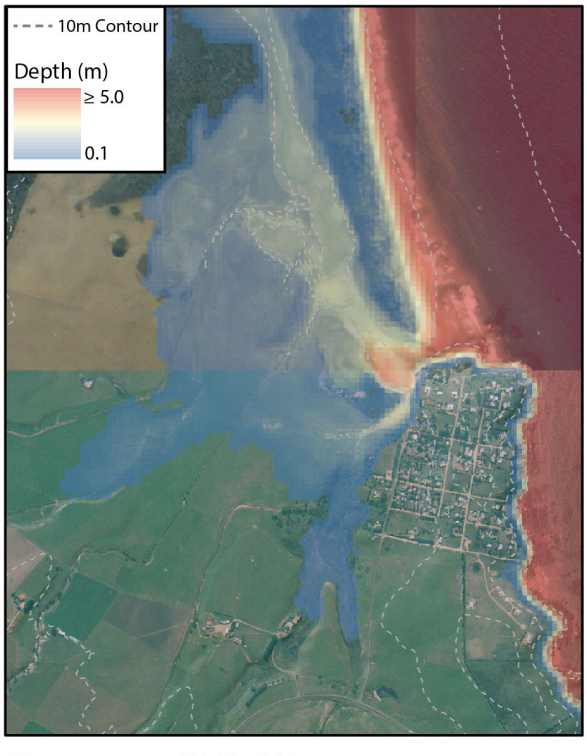

Puysegur - PU3679

FIGURE 21: Modelled tsunami inundation around Falmouth, for the four designated tsunami scenarios.

St Helens - Binalong Bay - Iarapuna (Bay of Fires) (Maps 30-38)

Modelled tsunami inundation patterns are similar for exposed parts of this coastal stretch, with incoming wave amplitudes of up to 4.5-5 m on the open coast (Figure 22), leading to flooding of beaches and lagoon areas. However, tsunami waves are attenuated within Georges Bay due to the protection offered by St Helens point and bar.

Simulated tsunami inundation at St Helens is generally less significant than towns in open coastal locations. Minor flooding of properties on the immediate shoreline could be expected, but most of the town centre and residential areas are outside the simulated tsunami footprint (Figure 23). However, more extensive inundation of low-lying areas north of St Helens is apparent in the modelling results (flow depths up to 1.5 m). This area includes tourist accommodation providers and residences along Binalong Bay Road, and industrial properties along Aquaculture Drive such as seafood processing plants and St Helens sewage treatment plant (Figure 24). Flooding of rural properties and land at Moulting Bay and Tuckers Arm could also be expected.

Inundation is relatively minor immediately east of St Helens but becomes more significant towards St Helens Point. Limited inundation occurs at low lying areas along St Helens Point Road, particularly around Boggy Creek, O'Connors Beach and around Steiglitz. Significant inundation is modelled at Maurouard Beach, with flow depths of up to 4 m and flooding reaching several hundred metres inland from the beach. Across the channel, Dora Point campground is also in the inundation zone.

Simulated wave amplitudes are relatively subdued within Georges Bay (less than 2 m, Figure 25). Modelled current speeds are variable, with speeds of 2.5–8.5 ms^{-1} simulated in the channel and bar area, and 0.5 - 1.75 ms^{-1} inside the embayment (see map series for details). These current speeds, combined with tsunami sediment disturbance or siltation, could have implications for aquaculture industries and ecosystems in the St Helens IBA. Significant erosion was modelled in the bar area, channel, and St Helens IBA.

Like the coastal communities farther south, most of the Binalong Bay residential area is located on a high rocky promontory that is above the maximum tsunami run-up height. However, flooding of low-lying areas around the margins of Grants Lagoon and Binalong Bay beach would be likely, which includes a number of campgrounds and tourist accommodation properties. Maximum incoming wave amplitude at this end of the study area is 5 m and flow depths on shore are ≤ 1.5 m.

Farther north, several camping sites and small roads in the Iarapuna (Bay of Fires) area are within the inundation footprint. However, flow depths are generally ≤ 1 m. Maximum incoming wave amplitudes in this area are generally 4-4.5 m.

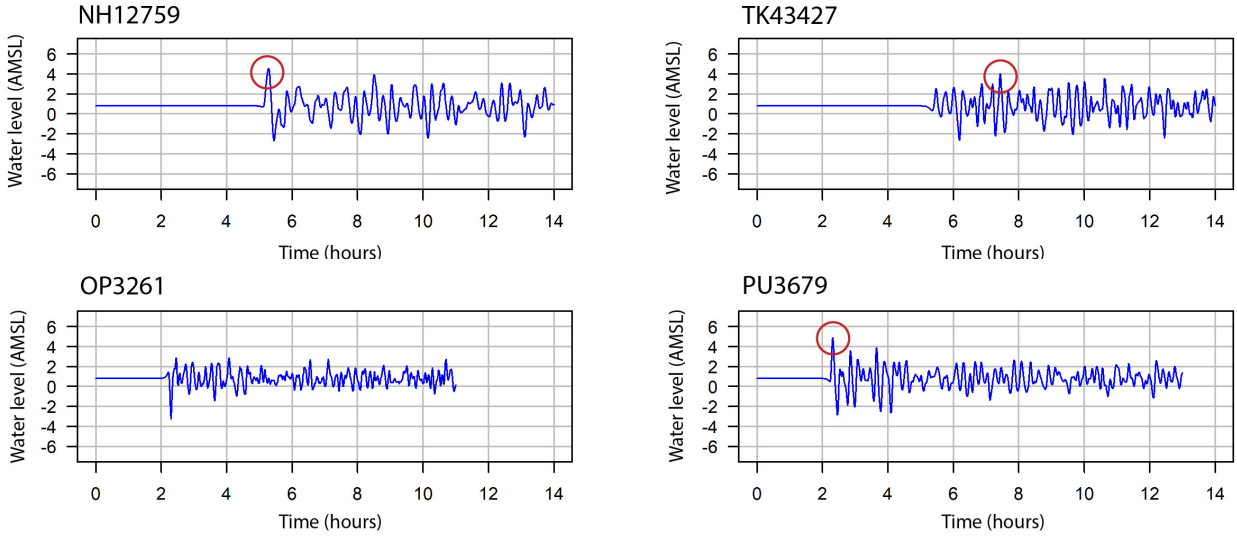

FIGURE 22: Simulated tsunami time series at Iarapuna (Bay of Fires). Maximum amplitude is circled in red.

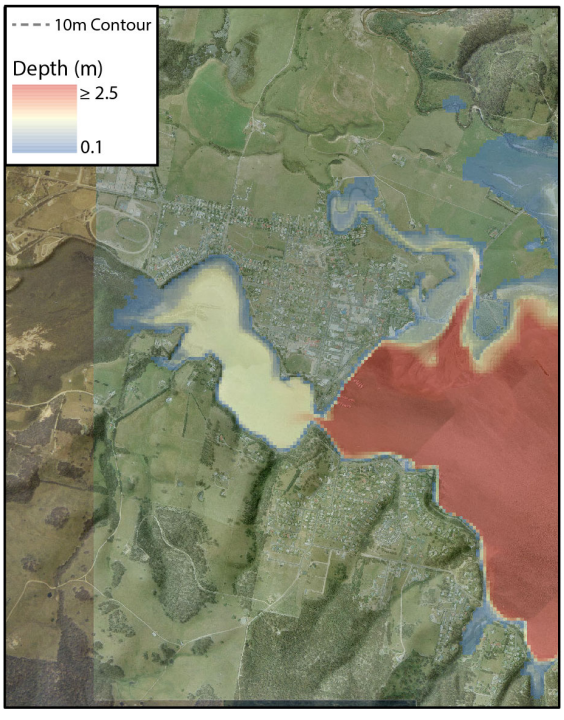

New Hebrides (NH3)

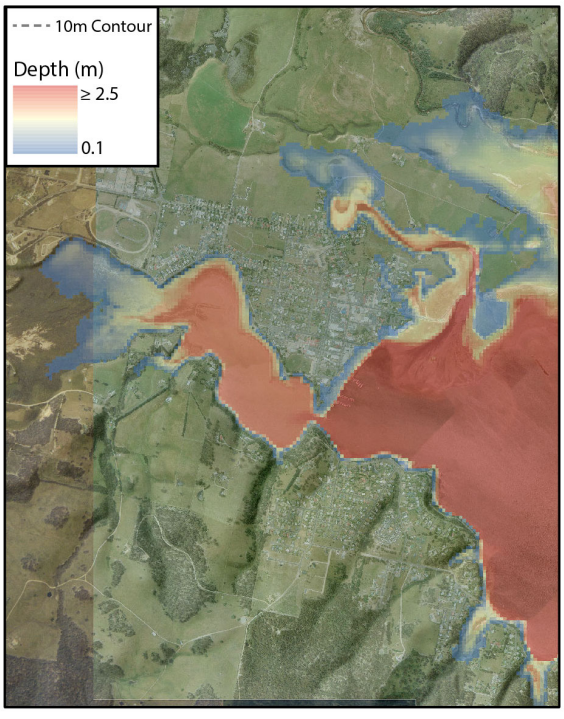

Tonga-Kermadec (TK4)

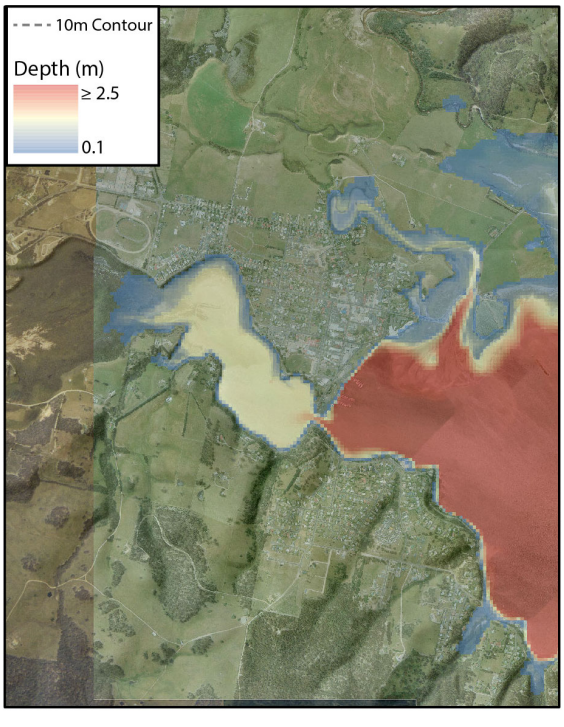

Outer Puysegur (OP2)

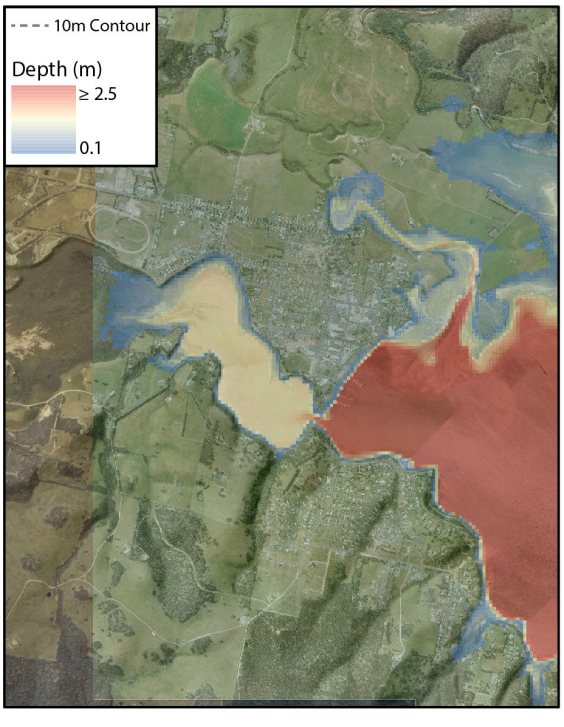

Puysegur (PU3)

FIGURE 23: Modelled tsunami inundation around St Helens for the four designated tsunami scenarios.

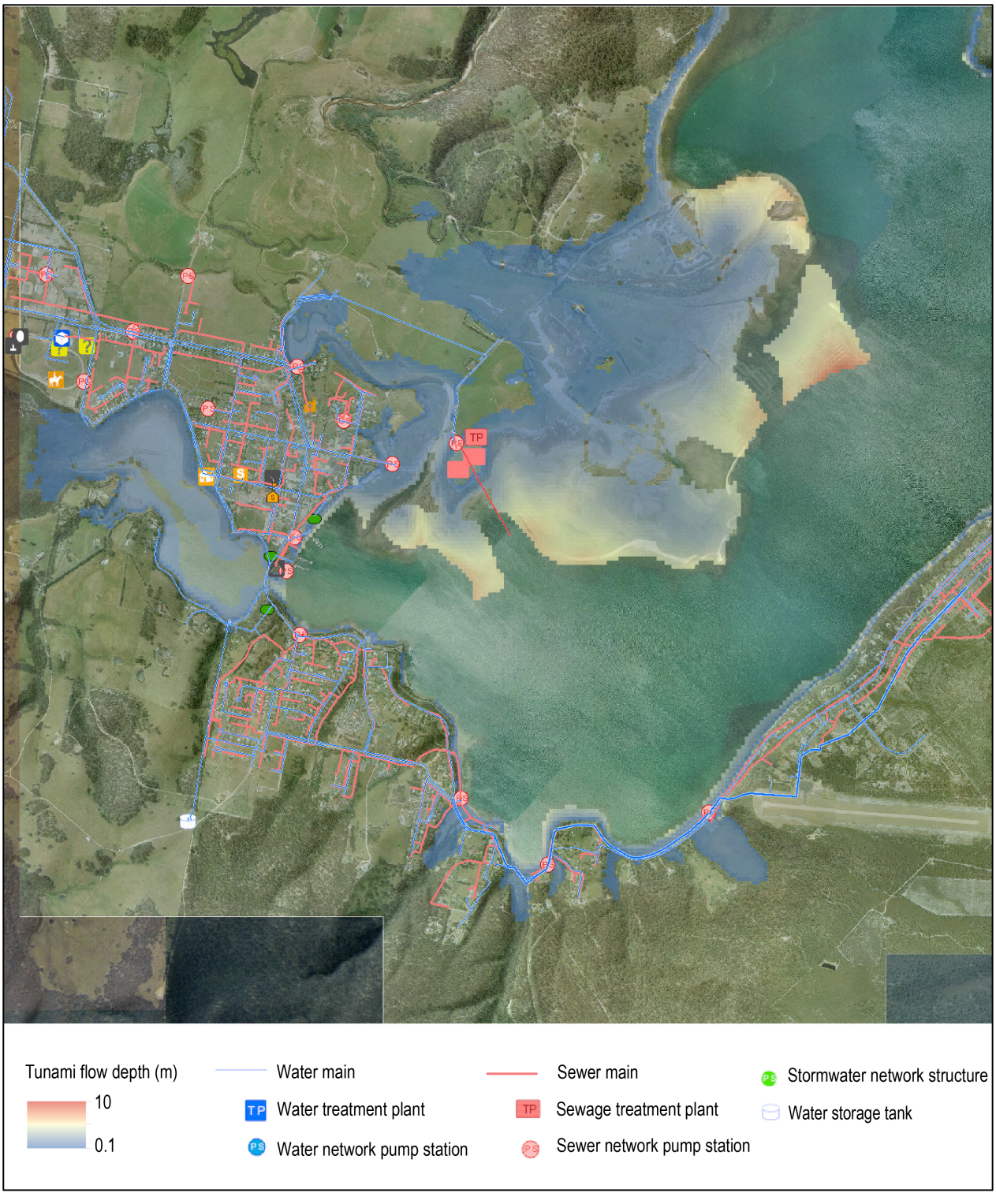

FIGURE 24: Map of infrastructure in the flooding zone at St Helens. Data from ListData (2019).

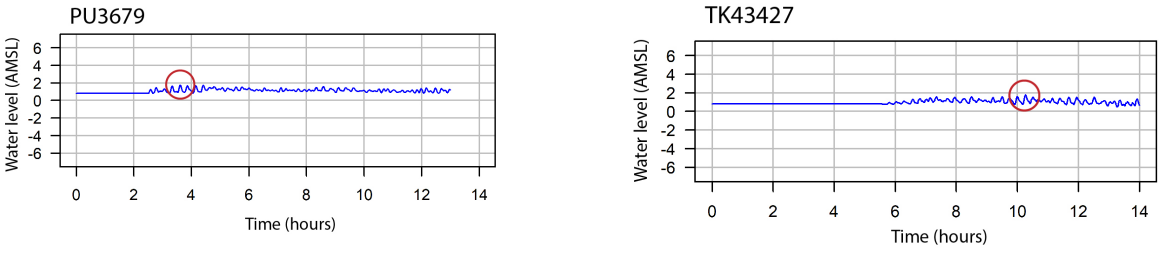

FIGURE 25: Simulated tsunami time series at St Helens township, highlighting the magnitude of wave attenuation within Georges Bay when compared with Figure 22. Maximum amplitude is circled in red.

Ansons Bay - Stumpys Bay

Simulated tsunami amplitudes are smaller along this stretch of coastline, reaching a maximum of approximately 4 m (Figure 26). However, the topography is relatively flat and so inundation patterns and maximum flow depths are similar to locations farther south.

The Ansons Bay township is largely protected from inundation in the simulations, with most of the tsunami energy reflected by the sandy barrier or attenuated as it passes through the bay entrance at Policemans Point. However, some inundation of waterfront properties could be expected, with flow depths of < 1 m (Figure 27).

The area north of Eddystone Point is characterised by sandy beaches and a number of campsites. Run-up in these areas reaches 7 m AMSL and extends up to 300 m inland around rivers, with flow depths of up to 4 m in beachside areas.

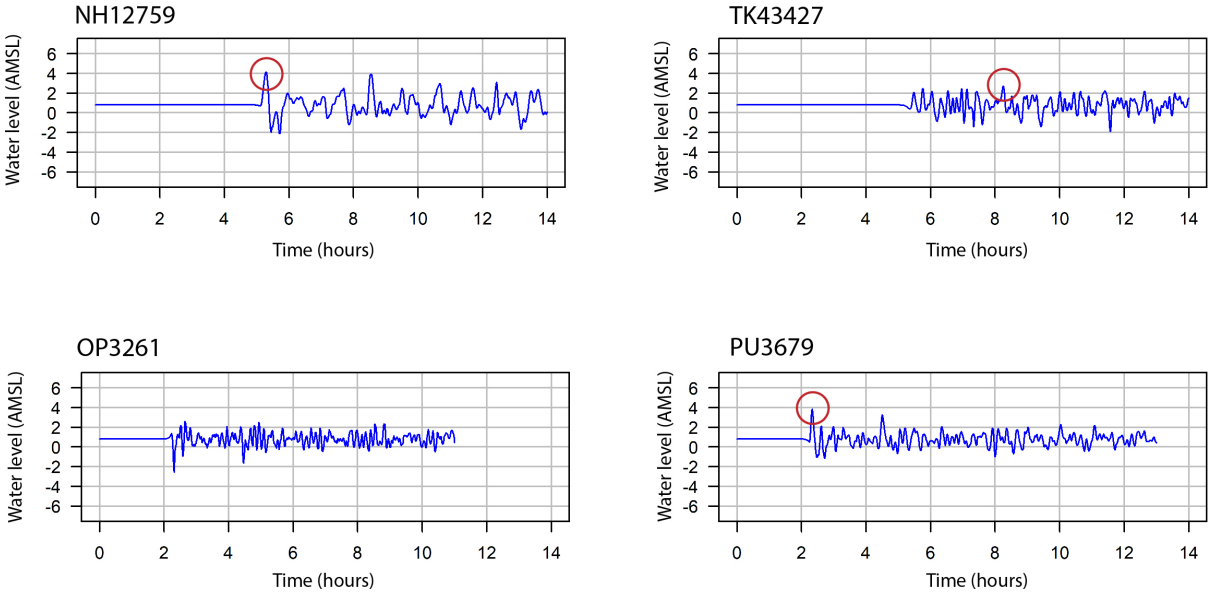

FIGURE 26: Simulated tsunami time series at Policemans Point, near Ansons Bay. Maximum amplitude is circled in red.

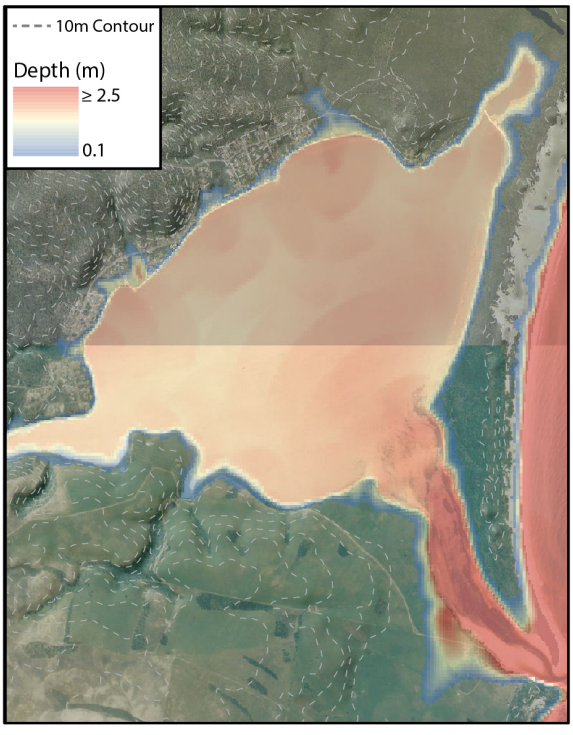

New Hebrides - NH12759

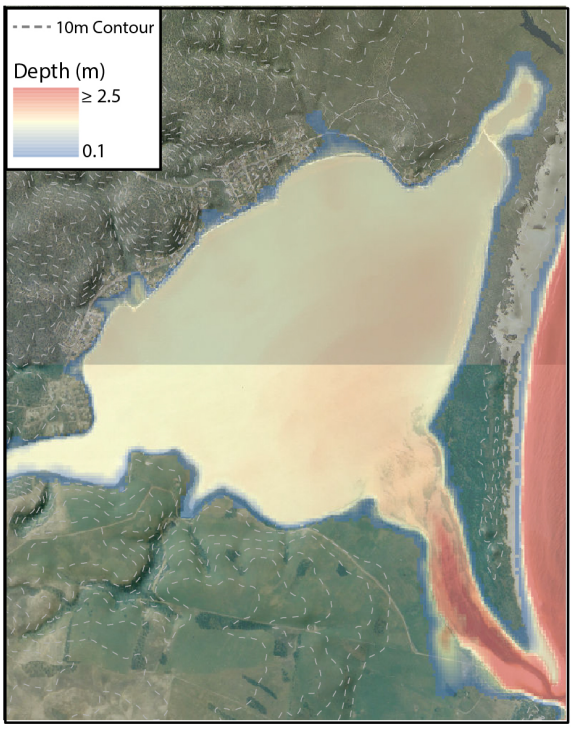

Tonga-Kermadec - TK43427

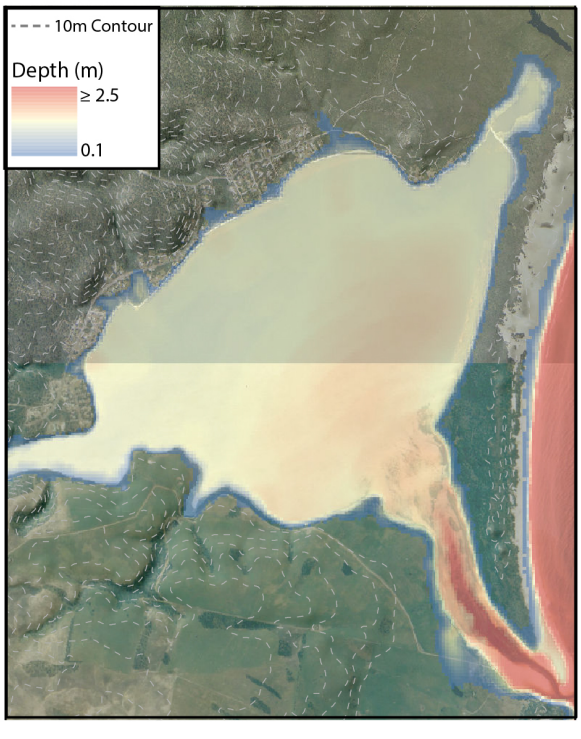

Outer Puysegur - OP3261

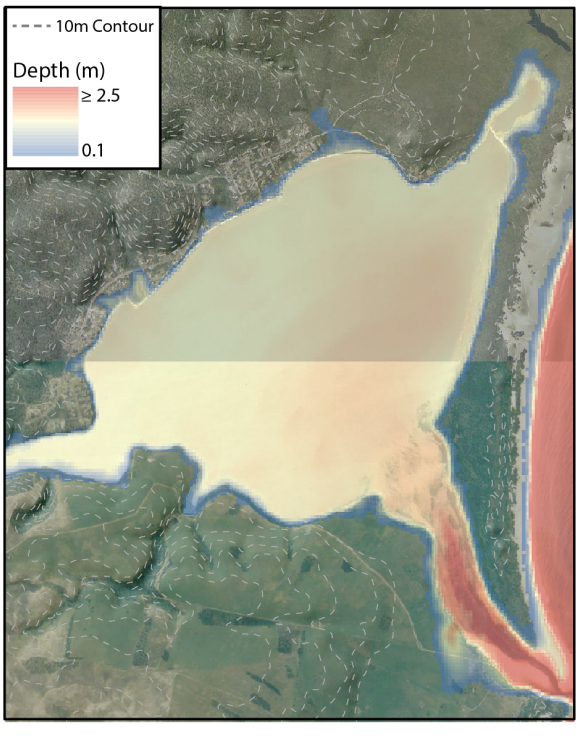

Puysegur - PU3679

FIGURE 27: Modelled tsunami inundation around Ansons Bay for the four designated tsunami scenarios.

DISCUSSION

Comparison between scenarios and source zones

In comparison with south east Tasmania, simulated inundation footprints and flow depths are generally less severe. The maximum tsunami stage (i.e. wave amplitude) at the 100 m depth contour for an ARI 10 000 year tsunami generally decreases from south to north, which suggests that the offshore tsunami hazard also decreases from south to north. For example, the PTHA maximum stage (equivalent to the tsunami amplitude) at the 100 m depth contour for an ARI 10 000 year tsunami is 2.61 m off Hobart but only 1.97 m off the coast of Scamander and 1.49 m at the northern model boundary. This difference can be explained by the particularly efficient capacity of the Puysegur Trench to propagate tsunami energy towards south east Tasmania, due to the orientation and dip angle of the subduction interface (Davies and Griffin, 2018).

Inundation footprints and maximum run-up heights are broadly similar for the four scenarios that were studied in detail. This is not unexpected, as all four scenarios have an ARI of approximately 11 000 years. The ARI for a given tsunami is defined in the PTHA by the maximum stage at a given hazard point, across all source zones, and so the scenarios were all of a similar maximum size at the 100 m depth contour. Secondly, the coastline in the model domain is mostly open and uncomplicated by inlets and islands, so differences in tsunami directionality and wave timing do not cause significant differences in impacts. The main exception to this is Great Oyster Bay, where energy propagation direction is more important due to the protection afforded by Freycinet Peninsula. Thirdly, the wave periods and thus the wavelengths of the tsunamis were also similar, which is important in confined areas like St Helens, where water can become backed up and tsunami waves amplified under certain conditions.

The results were again consistent when comparing all 20 scenarios (see Appendix 3 – multi-scenario map series for scenario footprints). Most scenarios ranged in ARI from 8000 to 16 000 years, with two "beyond-reasonably-credible" outliers (one from the Puysegur Trench and one from the Tonga-Kermadec Trench) of approximately 39 000 and 31 400 years respectively. These extreme scenarios were initially used for model sensitivity testing, but, as they too were run on a full-resolution mesh, the results provided an interesting insight into maximum inundation envelopes. In addition to the specific examples provided in the Results section of this report, there are a significant number of locations where the inundation limit for the most extreme scenario (Puysegur 3531, ARI = 39 000 years) was exceeded by multiple tsunamis with ARIs of 13 000 years or less. This observation highlights the importance of considering a range of scenarios when performing tsunami hazard and risk analysis. It would be interesting to test such relationships for smaller tsunamis, particularly around the threshold for land versus marine-only threat levels.

When comparing the results by source zone at a regional scale, there are three general trends. Puysegur tsunamis tend to result in slightly greater wave amplitudes and flow depths in the south of the study area when compared with other source zones, with impacts becoming less towards the north. The opposite is true for tsunamis generated on the New Hebrides Trench. These tsunamis tend to have slightly greater amplitudes and flow depths than Puysegur tsunamis in some northern locations (e.g. Scamander and Ansons Bay, with impacts decreasing southwards. Townships within Great Oyster Bay also seem to be somewhat sheltered from the full force of New Hebrides tsunamis by the Freycinet Peninsula. Tsunamis generated along the Tonga-Kermadec Trench show no clear spatial trends in terms of amplitudes and flow depths.

A comparison of time series data further highlights the importance of considering a range of scenarios, since nearshore tsunami behaviour cannot be predicted solely by the offshore tsunami amplitude (with the term ARI used here as a proxy for offshore tsunami amplitude). At the Bay of Fires for example, NH12551 and PU3574 both have an ARI of 9100 and result in maximum simulated tsunami amplitudes of 4.7 and 4.9 m respectively, whereas TK43665 has an ARI of 10 300 years but only causes a 3.8 m tsunami at this location. Similarly, at Scamander, a maximum tsunami amplitude of 5.1 m (first wave is attained for four different scenarios, ranging in ARI from 8800 to 13 400 years.

Time series graphs for some scenarios show large waves arriving late in the simulation at several locations. All scenarios show several large waves arriving over the 12-16 hour period following the first wave arrival, although only a few scenarios

show late waves of a comparable magnitude to the first one or two. The coastal time series were checked against the boundary condition time series to ensure this was a true representation of the tsunami as modelled by Geoscience Australia's propagation modelling, and not the result of spurious waves introduced by artefacts or wave reflection off the model boundary (i.e. poor model design). In all cases, these peaks were also present in the boundary condition time series and can be considered valid. Indeed, this phenomenon is commonly observed in tide gauge data and anecdotal records of large tsunamis elsewhere. However, it is important to note that the models become less accurate for long lead-in times, and later waves in the time series cannot be modelled as accurately as earlier arriving waves, due to the increasing importance of friction and shallow water interactions at later time steps (Davies and Griffin, 2018; Davies et al., 2020).

Limitations and recommendations

The modelling was not performed using a dynamic tide. The tidal level was set at HAT for the duration of the model simulation, which does not account for the interaction of tsunami waves with tidal currents and water level fluctuations. Ignoring tidal influence is particularly problematic over long timeframes and in confined areas like St Helens, but it is hoped that the use of HAT provides the most conservative estimate of tsunami inundation.

The mesh design means that vertical, or near-vertical, slopes are not well resolved in the model. Because the surface slope is assumed to be linear between mesh elements, the resolution of steep elements like riverbanks and coastal cliffs is limited by the mesh size. This problem could be mitigated by using break lines in ANUGA, but this solution was not feasible for a model of such size and complexity. In isolated areas like the cliffs around Freycinet Peninsula, this problem results in anomalously high tsunami run-up heights and flow depth values. These problems do not affect any populated areas and can be easily identified in the map series as small, contained pixels of high inundation occurring on cliffs, wharves, or steep banks.

The scope of this study does not extend to a tsunami risk assessment, which would require a detailed analysis of likelihood and consequence for a range of tsunami scenarios. This project is intended to be a deterministic, rather than probabilistic, study and as such focuses on the impacts of very rare tsunamis. Further work is recommended to help constrain the impacts of smaller and more likely tsunamis for Tasmania's east coast, as modelling of smaller events has been extremely limited. One smaller (marine threat threshold) tsunami has been modelled in south east Tasmania (Greenslade et al., 2019), but further modelling of a range of events is needed to better constrain land inundation thresholds on a more localised scale. In line with studies undertaken elsewhere in Australia (Boswood et al., 2013, 2018), tsunami events with an ARI of 750, 1000 and 3000 years could be useful.

A full analysis of the vulnerability of properties and infrastructure was also outside the scope of this project. However, a limited GIS analysis was undertaken at Scamander and St Helens as part of the 2021 update to the Tasmania State Disaster Risk Assessment (TASDRA), and is included in the results sections. Additionally, areas where one or more of the modelled tsunamis reached the A3 Tasman Highway were mapped and a GIS layer of these locations is provided in Appendix 6. Further GIS analysis is recommended to identify and quantify potential impacts on communities, infrastructure, and environmental processes.

The modelling was performed using the best available data. However, changes in elevation and land cover may affect how a tsunami would behave. These changes are particularly likely around mobile landforms such as dune systems and river mouth bars. In addition, the impacts of sea level rise and climate change are not directly accounted for in this model. Studies suggest that tsunami impacts could be increased significantly by even a modest sea level rise (Nagai et al., 2020; Yavuz et al., 2020); for example, Li et al., (2018) predict that tsunami hazard in Macau would double with a sea level rise of only 0.5 m. Climate change is also expected to result in more frequent and intense high water level events along Tasmania's coast (McInnes et al., 2012; Sharples, 2006). Erosion resulting from such storms would allow increased tsunami penetration in the event of a tsunami occurring before the beach had recovered.

SUMMARY AND CONCLUSIONS

The objective of this project was to improve understanding of the potential impacts of a critical-but-credible earthquake/tsunami/high tide scenario in eastern Tasmania. It builds upon previous work done in south east Tasmania by Geoscience Australia (Van Putten et al., 2009) and Kain et al. (2018). Tsunami inundation modelling was undertaken for 20 scenarios from three tsunami source zones: Puysegur Trench, Tonga-Kermadec Trench, and New Hebrides Trench. Deterministic exposure mapping was completed for 43 coastal locations from Swansea to Ansons Bay.

Modelling was undertaken using the 2-dimensional ANUGA hydrodynamic modelling library, applying a flexible triangulated mesh, variable surface roughness model, and dune erosion operator. Boundary condition data were obtained from the 2018 Probabilistic Tsunami Hazard Assessment (PTHA).

Modelled tsunami impacts were generally greater in the south, with Puysegur scenarios resulting in slightly greater flow depths and wave amplitudes in the south and New Hebrides scenarios dominating in the north. Tsunami travel times for Puysegur scenarios were approximately 2 hours 10 minutes post-earthquake, whereas travel times for Tonga-Kermadec and New Hebrides tsunamis were 5 hours 25 minutes and 5 hours 10 minutes, respectively. Maximum incoming tsunami wave amplitudes reached > 7 m AMSL in the south of the study area and 5 m AMSL in the north, whereas onshore run-up heights reached 7 m AMSL in exposed southern and central locations. Inundation footprints were topographically controlled in many locations and thus similar for all scenarios; however, simulated flow depths were generally greater for larger tsunamis. Many settlements are located > 8 m AMSL and were unaffected in the simulations. The greatest modelled flooding extents occurred in Scamander and Douglas River, with St Helens, Beaumaris and Bicheno also experiencing some impact on urban properties and infrastructure. Inundation of beach areas and low-lying coastal reserves was commonly observed along the entire coast, with campgrounds in areas such as Iarapuna (Bay of Fires) and Chain of Lagoons affected.

The results of this study do not constitute a tsunami risk assessment, but are intended to assist in the development of emergency management plans and procedures. A full risk assessment would require many more scenarios of varying magnitudes to be modelled, and a full analysis of vulnerability and exposure to be undertaken. Recommendations of this study include further work to quantify the risk in terms of vulnerable people, assets and infrastructure, and additional modelling of smaller tsunamis to better understand localised land inundation thresholds.

Changes in elevation and land cover may also affect the applicability of the results to future events, and as the models were run with a fixed tide height, the interaction of tsunami waves with tidal water levels and currents was not captured. The impacts of climate change and sea level rise were also not modelled; however, sea level rise could increase tsunami flow depths in low-lying areas and result in a greater susceptibility to inundation.

Alongside this report, the project outputs include two tsunami inundation map series sets, which cover 43 coastal communities and important reserve areas. These outputs are intended to assist emergency managers in understanding potential tsunami hazard along Tasmania's east coast.

ACKNOWLEDGEMENTS

This project was funded by a grant from the Natural Disaster Risk Reduction Grants Programme (NDRRGP), in conjunction with Mineral Resources Tasmania. Thank you to Ted Rigby from Rienco Consulting for valuable technical support and review.

REFERENCES

Australian Bureau of Statistics. (2016). Regional Population Growth, Australia, 2017–2018. https://www.abs.gov.au/AUSSTATS/abs@.nsf/mf/3218.0. Accessed 23 Aug 2019.

Australian Disaster Resilience Tsunami hazard modelling guidelines (AIDR, 2018). https://knowledge.aidr.org.au/media/5640/tsunami-planning-guidelines.pdf. Accessed 12 Dec 2020.

Ball J, Babister M., Nathan R., Weeks W., Weinmann E., Retallick M., Testoni I. (Editors) (2019). Australian Rainfall and Runoff: A Guide to Flood Estimation. Commonwealth of Australia (Geoscience Australia), 2019.

Boswood, P.K. (2013). Tsunami Modelling along the East Queensland Coast, Report 2: Sunshine Coast. Brisbane: Department of Science, Information Technology, Innovation and the Arts, Queensland Government.

Boswood, P.K., Wall, R., Peach, L. (2018). Tsunami Modelling along the East Queensland Coast, Report 3: Moreton Bay. Brisbane: Department of Environment and Science, Queensland Government.

Clark, K., Cochran, U., Mazengarb, C. (2011) Holocene coastal evolution and evidence for paleotsunami from a tectonically stable region, Tasmania, Australia. The Holocene 21, 883–895.

Davies, G., Griffin, J. (2018). The 2018 Australian probabilistic tsunami hazard assessment: hazard from earthquake generated tsunamis. Geoscience Australia, Record 2018/41. https://doi.org/10.11636/Record.2018.041.

Davies, G., Romano, F., Lorito, S. (2020). Global dissipation models for simulating tsunamis at far-field coasts up to 60 hours post-earthquake: Multi-site tests in Australia. Frontiers in Earth Science. https://doi.org/10.3389/feart.2020.598235.

Department of Police, Fire and Emergency Management (2017). Tasmanian Emergency Risk Assessment Guidelines TERAG Version 1.0. 96 pp.

Department of Primary Industries, Parks, Water and Environment (DPIPWE). (2007). LIST Tasmania 25 metre Digital Elevation Model. http://listdata.thelist.tas.gov.au/opendata/index.html#LIST_Tasmania_25_Metre_Digital_Elevation_Model. Accessed 20 April 2019.

Department of Primary Industries, Parks, Water and Environment (DPIPWE). (2015). LIST Tasmania Coastline. https://data.thelist.tas.gov.au/datagn/srv/eng/main.home?uuid=c10ccd03-dd2d-492d-8c2f-fca25baed194. Accessed 20 April 2019.

Department of Primary Industries, Parks, Water and Environment (DPIPWE). (2013). TASVEG 3.0: Tasmanian vegetation monitoring and mapping program. Resource Management and Conservation Division.

Fernandes, M. A. G. (2009). Systematic comparison on the inundation response of AnuGA and COMCOT tsunami modelling codes applied to the Boca do Rio and Alvor Bay area. Unpublished PhD Thesis, Univerisidade do Algarve. 75 pp.

Froelich, D. (2002). IMPACT project field tests 1 and 2 "Blind" simulation. 2nd IMPACT Project Workshop, Mo I Rana Norway.

Geoscience Australia (2018). PTHA Access. https://github.com/GeoscienceAustralia/ptha. Accessed 27 July 2021.

Greenslade, D.J.M., Uslu, B., Allen, S.C.R., Kain, C.L., Wilson, K.M., Power, H.E. (2019). Evaluation of Australian tsunami warning thresholds using inundation modelling. Pure and Applied Geophysics 177, 1425-1436.

Jakeman, J. D., Nielsen, O. M., Van Putten, K., Mleczko, R., Burbidge, D., & Horspool, N. (2010). Towards spatially distributed quantitative assessment of tsunami inundation models. Ocean Dynamics, 60, 1115–1138.

Kain, C.L., Mazengarb, C. (2020). Construction of the Statewide Digital Terrain Model (DTM) for Tasmania. Geological Survey Technical Report 22, Mineral Resources Tasmania.

Kain, C. L., Mazengarb, C., Rigby, E. H., Cohen, B., Simard, G., & Lewarn, B. (2018). Technical report on tsunami inundation modelling in South East Tasmania. Tasmanian Geological Survey Report UR2018_02. 160 pp.

Kain, C.L., Lewarn, B., Rigby, E.H., Mazengarb, C. (2019). Tsunami inundation and maritime hazard modelling for a maximum credible tsunami scenario in southeast Tasmania, Australia. Pure and Applied Geophysics 177, 1549-1568.

Keith, 1868. Note from Overseer to Commandant, Mitchell Library NSW. Tas Papers 315, pp 657-659.

Land Information System Tasmania. (2019). ListData Open data. https://listdata.thelist.tas.gov.au/opendata/ Accessed 12 April 2019.

Li, L., Switzer, A.D., Wang, V., Chan, C., Qiu, Q., Weiss, R. (2018). A modest 0.5-m rise in sea level will double the tsunami hazard in Macau. Science Advances 4 (8) doi: 10.1126/sciadv.aat1180.

Lucieer, V. (2007): SeaMap Tasmania Bathymetric Data. Institute for Marine and Antarctic Studies, University of Tasmania dataset.

McInnes, K.L., O'Grady, J.G., Hemer, M., Macadam, I., Abbs, D.J., White, C.J., Corney, S.P., Grose, M.R., Holz, G.K., Gaynor, S.M., Bindoff, N.L. (2012). Climate Futures for Tasmania: extreme tide and sea-level events technical report, Antarctic Climate and Ecosystems Cooperative Research Centre, Hobart, Tasmania.

Morris, M.K., Mazengarb, C. (2009). Historical accounts of tsunamis in Tasmania. Tasmanian Geological Survey Record 2009/04. Department of Infrastructure, Energy and Resources, Mineral Resources Tasmania.

Mount, R., Crawford,C. Veal, C., White, C. (2005). Bringing Back the Bay: Marine Habitats and Water Quality in Georges Bay, Break O'Day Natural Resource Management Strategy, Hobart. 102 pp.

Mungkasi, S., Roberts, S.G. (2013). Validation of ANUGA hydraulic model using exact solutions to shallow water wave problems. Journal of Physics: Conference Series 423, 012029. https://doi.org/10.1088/1742-6596/423/1/012029.

Nagai, R., Takabatake, T., Esteban, M., Ishii, H., Shibayama, T. (2020). Tsunami risk hazard in Tokyo Bay: The challenge of future sea level rise, International Journal of Disaster Risk Reduction 45 https://doi.org/10.1016/j.ijdrr.2019.101321.

Nielsen, O., Roberts, S., Gray, D., McPherson, A., & Hitchman, A. (2005). Hydrodynamic modelling of coastal inundation. MOD-SIM 2005 In: International Congress on Modelling and Simulation, Modelling and Simulation Society of Australia & New Zealand, pp. 518–523.

Rigby, E., Mazengarb, C., Barthelmess, A., Kain, C. (2017). Experiences developing and applying an ANUGA dune erosion operator to assess risk from loss of dune protection during a tsunami. Proceedings of the 13th Hydraulics in Water Engineering Conference (14-16 November, 2016).

Roberts, S., Nielsen, O., Gray, D., Sexton, J., & Davies, G. (2019). ANUGA user manual. Geoscience Australia. https://anuga.anu. edu.au/

Satake, K., Heidarzadeh, M., Quiroz, M., Cienfuegos, R. (2020). History and features of trans-oceanic tsunamis and implications for paleo-tsunami studies. Earth-Science Reviews 202. 103112.10.1016/ j.earscirev.2020.103112.

Sharples, C. (2006). Indicative mapping of Tasmanian coastal vulnerability to climate change and sea-level rise: explanatory report, Consultant Report to Department of Primary Industries & Water, Tasmania, Second edition. 173 pp.

Van Putten, K., Fountain, L., Griffin, J., Sexton, J., Nielsen, O., Wilson, R. (2009). Capacity building for tsunami planning and preparation: inundation models for south east Tasmania. Geoscience Australia Professional Opinion. No.2009/07. Geoscience Australia: Canberra.

White, C.J., Remenyi, T., McEvoy, D., Trundle, A., Corney, S.P. (2016). 2016 Tasmanian State Natural Disaster Risk Assessment: All Hazard Summary, University of Tasmania, Hobart.

Whiteway, T. (2009). Australian bathymetry and topography grid, June 2009. Scale 1:5 000 000. Geoscience Australia : Canberra.

Williams, J.H., Wilson, T.M., Horspool, N., Lane, E.M., Hughes, M.W., Davies, T., Le, L., Scheele, F. (2019). Tsunami impact assessment: development of vulnerability matrix for critical infrastructure and application to Christchurch, New Zealand. Natural Hazards 96, 1167–1211.

Yavuz, C., Kentel, E., Aral, M.M. (2020). Climate Change Risk Evaluation of Tsunami Hazards in the Eastern Mediterranean Sea. Water 12(10), 2881 https://doi.org/10.3390/w12102881.

GLOSSARY

AEP	Annual Exceedance Probability. The likelihood of occurrence of a tsunami of given size or larger occurring in any one year. AEP is expressed as a percentage (%) and may be expressed as the reciprocal of ARI (Average Recurrence Interval)
AHD	Australian Height Datum – approximate mean sea level (MSL)
ANUGA	A free and open source hydrodynamic modelling library developed by the Australian National University (ANU) and Geoscience Australia (GA)
ARI	Average Recurrence Interval. The likelihood of occurrence, expressed in terms of the long-term average number of years, between tsunami events as large as or larger than the designated tsunami event. ARI (in years) is the reciprocal of AEP (events per year)
Bathymetry	The depth of the ocean floor from the water surface (mean sea level)
Boundary conditions	Locations in the model where water flows into or out of the model domain
Flow depth	The depth of the tsunami water onshore
HAT	Highest Astronomical Tide – the highest water level that can be predicted to occur under any combination of astronomical conditions
LAT	Lowest Astronomical Tide – the lowest water level that can be predicted to occur under any combination of astronomical conditions
LiDAR	Light Detection and Ranging – a laser remote sensing system used to collect topographic data
Manning's *n*	A model input parameter representing surface roughness, i.e. a measure of the amount of frictional resistance water experiences when passing over land and channel features
Maximum current speed	The maximum induced current speed at a given location across the duration of the tsunami simulation
Maximum wave height	The distance from peak to trough (at a given location) of the wave that generated the highest water level across the duration of the tsunami simulation
MSL	Mean Sea Level. The arithmetic mean of hourly heights of the sea at the tidal station observed over a period of time
Mw	Moment magnitude of an earthquake
Palaeotsunami	A tsunami that occurred prior to written historical records. Usually identified by signatures left in the geological record
Run-up height	The maximum elevation (above AHD) reached by the uprush of the tsunami onto land
Stage or stage height	The level of the water surface above mean sea level
Subduction zone	A region of the Earth where two tectonic plates are converging and one plate is sliding beneath the other e.g. the Puysegur Trench
Topographic height	The elevation of the land surface above the Australian Height Datum stated in metres above AHD
Wave amplitude	The vertical distance between the crest of the tsunami and the still water level
Wave height	The vertical distance between the tsunami crest and trough. Approximately twice the wave amplitude.
Wave length	The distance between successive crests in a wave. In this case, it was approximated from the simulated velocity and 2 x the time period between the maximum peak and its associated trough

LIST OF APPENDICES

Appendix 1	Potential tsunami impacts on infrastructure	p A1-A4
Appendix 2	Tsunami Inundation Map Series	See accompanying volume
Appendix 3	Tsunami Inundation Multi-Scenario Map Series	See accompanying volume
Appendix 4	Time series and GIS data	Digital file - see data package
Appendix 5	Video animations of tsunami simulations	Digital file - see data package
Appendix 6	A3 Highway flooding locations	Digital file - see data package
Appendix 7	Modelling scripts and input data	Digital file - see data package

TECHNICAL REPORT ON TSUNAMI INUNDATION
MODELLING ON THE EAST COAST OF TASMANIA

Potential tsunami impacts on infrastructure

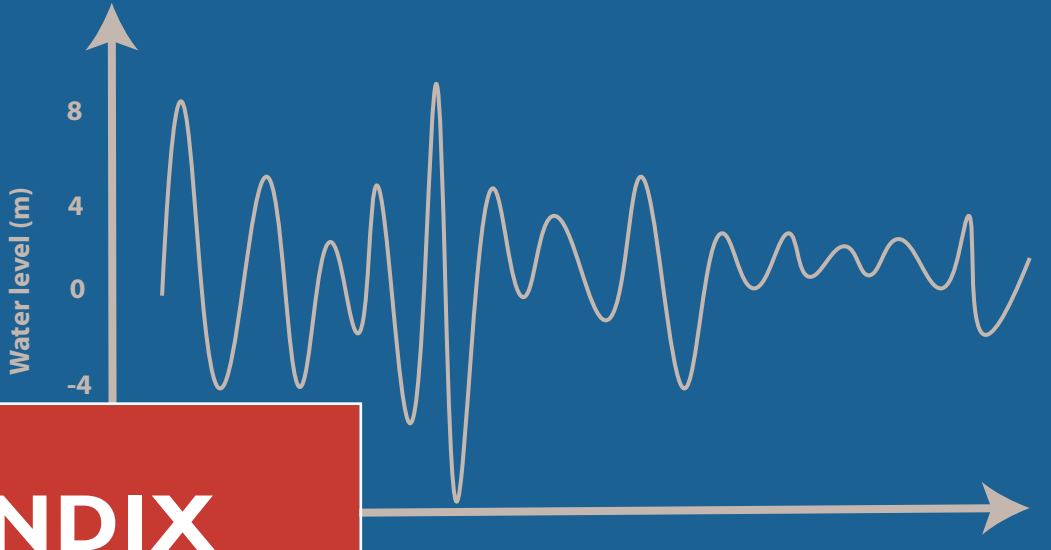

APPENDIX ONE

Mineral Resources Tasmania
Department of State Growth

Tasmanian Government

POTENTIAL TSUNAMI IMPACTS ON INFRASTRUCTURE

This table provides a breakdown of potential tsunami impacts on infrastructure, based on tsunami flow depth. The data in this table is not specific to Tasmanian settings, but was compiled by Williams et al. (2019) from a global literature review of tsunami risk assessments, modelling studies (including fragility models), and reports of actual tsunami damage.

Colour key:

Grey	No or negligible damage potential
Green	Low damage potential
Yellow	Medium damage potential
Orange	High damage potential

Critical infrastructure component	Tsunami flow depth < 0.5 m	Tsunami flow depth 0.5-2 m	Tsunami flow depth > 2 m
Roads	• Light sediment deposition • Water ponding	• Sediment or debris coverage • Scour of base materials • Destruction of signage and road markings • Water ponding	• Debris and sediment deposition • Scour of base materials • Lifting of carriageway • Destruction of barriers and signage • Cracking of pavement • Liquefaction of base materials • Water ponding
Bridges	• Superficial debris strikes • Light sediment deposition	• Bank erosion • Debris strikes • Sediment deposition • Scour of footings • Washout of light timber structures • Corrosion	• Debris and sediment deposition • Erosion of banks and scour of footings • Barriers destroyed or bent • Widening or aggradation of waterway • Separation of deck from footings • Distortion of structure • Corrosion • Loss of utilities across bridge
Vehicles	• Water incursion • Damage to electrical components	• Debris strikes and impact damage • Floating • Water incursion • Damage to electrical components	• Debris strikes and impact damage • Floating • Water incursion • Damage to electrical components

Buildings	• Water incursion • Damage to interiors and goods inside	• Water incursion • Damage to interiors and goods inside • Washout • Short circuiting of electrics	• Water incursion • Damage to interiors and goods inside • Washout • Short circuiting of electrics
Electricity - utility poles/overhead lines	Negligible impact	• Lines severed from pulling of utility poles • Shorting of inundated transformers • Scour of pole foundations	• Debris strikes • Lines severed • Short circuiting • Scour of pole foundations • Water damage • Shorting of transformers • Washout
Substations	• Light sediment deposition • Short circuit of low-lying electrical components	• Saltwater contamination of electrical components and structures • Debris and sediment deposition • Debris strikes • Building damage • Washout of some outdoor components	• Saltwater contamination of electrical components and structures • Debris and sediment deposition • Debris strikes • Building damage • Washout of some outdoor components
Storage tanks (e.g. petroleum, water)	Negligible impact	• Debris strikes • Buckling of tank base • Lifting of empty or small tanks • Scour of foundations	• Debris strikes and impact damage • Scour and/or liquefaction of foundations • Floating • Crushing • Loss of liquid inside
Water pumping stations (wastewater or freshwater)	• Inundation of low-lying electrical components • Water damage to electrical and mechanical equipment	• Failure of electrical and pumping equipment • Salt water and sewage contamination • Sediment and debris cover • Debris strikes	• Failure of electrical and pumping equipment • Salt water and sewage contamination • Sediment and debris cover • Debris strikes • Structural collapse • Washout
Wastewater treatment plants	• Saltwater contamination	• Sediment deposition • Erosion of embankments • Inundation of machinery and structures • Saltwater contamination of ponds, filters and pumps	• Sediment deposition • Erosion of embankments • Inundation of machinery and structures • Salt water contamination of ponds, filters and pumps

		• Spread of contaminants to surrounding area	• Washout of contaminants to surrounding area • Components exposed and washed away
Septic tanks and onsite wastewater systems	• Saltwater contamination	• Saltwater contamination • Floating of low-volume tanks • Scour of backfill	• Sediment infill • Floating of low-volume tanks • Scour • Localised contamination spread
Wastewater or freshwater pipes	• Minor siltation	• Exposure • Scour of weak backfill • Non-HDPE pipes severed • Damage to water meters	• Scour and exposure • Debris strikes • Bending, fracturing or severing • Decoupling at entry point to buildings or tanks • Siltation • Blockages • Some HDPE pipes severed • Damage to water meters
Drinking water wells	• Salt water contamination of shallow wells	• Saltwater and sewage contamination • Groundwater contamination • Debris strikes to components	• Salt water and sewage contamination • Groundwater and aquifer contamination • Scour • Debris strikes • Components exposed and washed away
Stormwater systems	• Sediment and/or debris infiltration • Blockage • Saltwater contamination	• Scour of embankments • Exposure of pipes • Siltation, sediment and debris blockage • Saltwater contamination • Damage to electrical components • Removal or damage to vegetation (e.g. wetland systems)	• Scour of embankments • Exposure of pipes • Siltation, sediment and debris blockage • Saltwater contamination • Damage to electrical components • Removal or damage to vegetation (e.g. wetland systems) • Widening of unreinforced channels • Covers lifted • Floating of low-volume tanks • Collapse of outflows
Irrigation (canals and storage)	• Debris blockage • Siltation/sediment deposition	• Debris blockage • Siltation/sediment deposition	• Debris blockage • Siltation/sediment deposition

	• Saltwater contamination	• Saltwater contamination • Scour of embankments • Removal or damage to vegetation	• Saltwater contamination • Scour of embankments • Removal or damage to vegetation
Coastal defences (seawalls, breakwaters)	Negligible impacts	• Scour of foundations	• Liquefaction and scour of foundations • Tilting of concrete blocks • Removal of materials, especially on back side of seawalls
Dunes and embankments	Negligible impacts	• Removal of vegetation • Erosion • Debris coverage	• Removal of vegetation • Erosion • Debris coverage • Washout • Migration or reorganisation of dunes
Telecommunications – transmission towers, switch boxes, exchange centres, cabling	• Scour of support base or backfill • Tilting of supports • Water damage to electrical components	• Scour and exposure of cables – particularly at entrance to buildings • Ducting and cables across waterways severed • Water damage/short circuiting of electrical components • Debris strike • Washout • Corrosion	• Scour and exposure of cables, particularly at entrance to buildings • Ducting and cables across waterways severed • Water damage/short circuiting of electrical components • Debris strike • Washout and collapse • Corrosion
Maritime hazard - vessels	• Broken moorings • Debris strikes	• Broken moorings • Debris strike and damage • Uncontrolled floating • Collisions	• Broken moorings • Debris strike and damage • Uncontrolled floating • Capsized • Submerged • Oil spill • Collisions
Maritime hazard – port infrastructure, wharves and piers	• Scour of foundations	• Sediment and debris deposition • Debris strikes • Scour of seabed and foundations • Debris in waterways	• Aggradation or erosion of seabed • Separation of deck slabs from footings • Removal of concrete blocks • Subsidence • Collapse • Washout • Debris in waterways

Mineral Resources Tasmania
PO Box 56 Rosny Park Tasmania 7018
Phone: (03) 6065 4800
Fax: (03) 6233 8338
info@mrt.tas.gov.au
www.mrt.tas.gov.au